IVYSPRING INTERNATIONAL PUBLISHER

JOURNAL OF CANCER

2026; 17(12): 2103-2125. doi: 10.7150/jca.143837

Review

# Lung Cancer Evolves as an Ecosystem from Niche Dysregulation to Metastasis and Treatment Resistance

Jie Wu[1], Youyi Ding[1], Peiliang Huang[1], Yan Chen[2], Shuo Chen[1]✉

1. Department of Pharmacy, Chaozhou Central Hospital, Chaozhou 521000, Guangdong Province, China.
2. Department of Hematology and Oncology, Chaozhou Central Hospital, Chaozhou 521000, Guangdong Province, China.

✉ Corresponding author: Shuo Chen, Email: Memecha16@163.com.

© The author(s). This is an open access article distributed under the terms of the Creative Commons Attribution License (https://creativecommons.org/licenses/by/4.0/). See https://ivyspring.com/terms for full terms and conditions.

Received: 2026.09.08; Accepted: 2026.10.24; Published: 2026.11.13

## Abstract

The clinical heterogeneity of lung cancer, the continuing divergence between primary and metastatic lesions, and relapse after treatment cannot be fully explained by a linear model of cancer-cell-intrinsic mutation. Most tumor-microenvironment reviews describe a local system at a single time point and rarely follow lung cancer across disease stages and organs. Here, we use the ecosystem as a unifying framework to examine how genetic change, tissue injury, immune remodeling, and stromal remodeling jointly drive tumor initiation, invasion, dissemination, and post-treatment evolution. We argue that lung cancer initiation is never the autonomous linear expansion of a single mutant cell; it is a systemic event shaped by genetic alteration, failed repair, and niche dysregulation. Fit clones remodel their habitat through metabolic adaptation, phenotypic plasticity, and immune regulation, creating a selectively permeable ecotone at the invasive front. An analogy with mangrove ecotones captures the asymmetric filtering of tumor-cell egress and immune-cell entry across this boundary. Cross-compartment dissemination then imposes serial bottlenecks, for which founder effects during human migration provide a structural analogy for non-random lineage sampling. Longitudinal multiregion studies further show that primary and metastatic lesions form dynamic source-sink networks in which metastases can become new seeding sources. Therapy both eliminates cancer cells and reorganizes competition, niche conditions, cell states, and mutational input, thereby shaping resistance and relapse. We propose operational definitions and a mathematical modeling framework for carrying capacity, habitat quality, and lesion output to extend assessment beyond shrinkage and inform multi-lesion sampling, source-lesion identification, and feedback-guided intervention.

Keywords: lung cancer; tumor ecosystem; niche construction; clonal evolution; source-sink network; therapy-driven selection

## Introduction

Molecular stratification, targeted therapy, and immune-checkpoint blockade have transformed lung cancer care, yet identical biomarkers do not ensure identical benefit. Different lesions in the same patient may show different drug sensitivities, and a single biopsy cannot explain mixed responses, organ-specific metastasis, or treatment-associated lineage switching. The cancer-cell genome is fundamental, but spatial position, immune state, stromal architecture, and drug accessibility also shape clinical outcome [1-3]. The updated hallmarks of cancer incorporate inflammation, phenotypic plasticity, and non-genetic reprogramming [4], while clonal evolution links genetic diversification to changing tissue-level selection pressures [5]. Whether an abnormal clone gains an advantage depends on niche dysregulation in the surrounding tissue, immune surveillance, competition for resources, and the clone's capacity to remodel that niche.

Most reviews of the tumor microenvironment are organized around cell types or signaling pathways. This approach identifies the components of lung cancer progression but is less suited to explaining how their interactions drive transitions between disease states. Single-cell and spatial studies now show that cell function emerges from neighborhood context and interaction networks and cannot be inferred from identity alone [6-11]. Lung cancer evolves as an open

ecosystem through continuous interactions with host tissue. Environmental filtering, competitive release, and niche construction connect chronic injury to clonal emergence; the ecotone concept resolves the invasive front; dispersal bottlenecks and founder effects explain cross-compartment dissemination; and metapopulation and source-sink dynamics reconstruct the network linking primary and metastatic lesions. Once therapy enters this system, it changes not only cancer-cell abundance but also competition, mutational input, immune architecture, and habitat quality, becoming part of the process that shapes relapse.

This review organizes dispersed microenvironmental mechanisms into a continuous trajectory from tissue injury and tumor initiation through local takeover, boundary advance, and distant colonization. It also shifts the analytical scale from the primary tumor to the patient-wide network of lesions. The resulting framework explains heterogeneity, organ selectivity, and post-treatment reconstruction while generating testable clinical propositions for multi-lesion sampling, identification of high-output lesions, organ-specific intervention, and feedback-guided ecological control.

## 1. Components, dynamics, and boundaries of the malignant ecosystem

### 1.1 From a mass of cancer cells to a host-dependent open system

An ecosystem comprises a biological community, its abiotic environment, and the continuing exchange of matter and information between them. Niche construction occurs when organisms modify their surroundings and thereby change the selection pressures acting on themselves and other organisms [12, 13]. Tumor cells, macrophages, lymphocytes, myeloid-derived suppressor cells, fibroblasts, and endothelial cells form a local community within the extracellular matrix (ECM). Oxygen, nutrients, pH, mechanical tension, blood flow, and drug gradients define the conditions in which this community operates. Single-cell and spatial atlases of the healthy human lung reveal stable compartmental organization among epithelial, immune, and stromal cells [6-8]. Tumor formation rearranges these boundaries, but the system remains dependent on host circulation, immunity, and organ function.

Spatial mosaicism is a defining structural feature of this ecosystem. Perivascular, hypoxic, matrix-dense, and invasive-front regions experience different pressures from resources, immunity, and treatment. Foundational work on microenvironmental regulation of tumor progression established that genetically stable host components can restrain tumors and can also be co-opted by them [9]. Single-cell and spatial transcriptomic analyses of small-cell lung cancer have linked CXCL12-CXCR4-dependent myeloid recruitment to an immune-desert phenotype [10], while spatial immune profiling in lung cancer shows that similar immune-cell densities do not confer equivalent access to cancer cells [11]. Spatial immune organization and vascular and stromal states are measurable features of the tumor ecosystem and potential targets for intervention.

This mosaicism makes the "average microenvironment" potentially misleading. A single lesion may contain inflamed, immune-excluded, and immune-desert regions, and neighboring regions separated by only a few hundred micrometers may experience markedly different oxygen, nutrient, and drug exposure because of vascular distance or collagen density. Immunohistochemical and transcriptomic averages flatten this structure, whereas a regional biopsy may mistake a local state for a property of the whole lesion. Ecological analysis links each cell state to its spatial location and local resource availability.

Feedback adds a temporal dimension to this structure. Abnormal vessels supply nutrients yet create heterogeneous perfusion and hypoxia; hypoxia induces metabolic reprogramming and angiogenesis while increasing acidic metabolites and immunosuppression. Matrix deposited by cancer-associated fibroblasts (CAFs) may constrain early expansion, then form migratory tracks and poorly perfused drug refuges as remodeling continues. Immune cells can eliminate malignant cells but may become exhausted or suppressive under chronic stimulation. As these local conditions change, the same components can restrain or support tumor growth.

### 1.2 Asymmetric co-evolution between tumor and host

Lung cancer progression reflects reciprocal interactions between evolving tumor clones and host tissue. Tumor clones modify immune, stromal, and vascular states through cytokines, metabolites, and extracellular vesicles. In turn, host hypoxia, inflammation, tissue mechanics, and resource availability select among clones. Spatial studies show that the adjacency of cancer cells to myeloid cells, lymphocytes, and fibroblasts can influence immune exclusion and local expansion [9-11]. These reciprocal feedbacks allow tumor and host to reshape one another throughout disease progression.

The two sides adapt by different means. Cancer cells commonly acquire heritable differences through

mutations, copy-number alterations, and chromosomal instability. Immune and stromal cells more often adapt through transcriptional, metabolic, and epigenetic reprogramming. Genetic diversification defines cancer-cell lineages, while host-cell reprogramming changes the selective environment. Stable genetic variation and reversible host-cell states can reinforce one another within the same feedback loop. Once a clone is better suited to exploit the current habitat, its expansion further alters that habitat and changes the conditions confronting later competitors [4, 5].

Chronic injury weakens the competitive capacity of normal tissue, after which abnormal clones hijack repair signals, co-opt stromal and immune cells, and progressively redirect local resources. Selection retains states that both tolerate damaged tissue and make the surrounding environment more supportive of their persistence.

### 1.3 Analytical scale, system boundaries, and observability

Tansley introduced the term ecosystem to place biological communities and their physical environment within the same functional system, and later work extended this view to critical zones spanning biological, geochemical, and physical processes [14, 15]. For lung cancer, the appropriate system boundary depends on the research question. A few hundred micrometers of invasive front may be the appropriate unit for studying local immune exclusion; analysis of metastasis must instead place the primary lesion, circulation, lymph nodes, and distant organs within one open network. As environmental drivers and interactions multiply, behavior becomes increasingly difficult to extrapolate from a single pathway. Food-web research on emergent complexity under multiple drivers offers a methodological analogy for this problem [16].

Scale also determines what an experiment can establish. The ECM can maintain dormancy and create poorly perfused regions, then support reawakening and invasion after remodeling. Three-dimensional culture can reconstruct selected cell-matrix-fluid relationships but lacks a complete immune system, organ physiology, and prior treatment history [17, 18]. Reviews of the lung cancer microenvironment and microenvironment-directed therapy have catalogued candidate interventions targeting CAFs, myeloid cells, abnormal vessels, and ECM [19, 20]. Redundancy and compensation in host physiology allow other supportive pathways to replace a blocked cell type or factor.

Vasculature and matrix jointly shape the functional conditions of the lung cancer habitat. Cellular genotype and ECM can regulate one another, and matrix can both restrain tumor expansion and shelter cancer cells [21, 22]. Abnormal vessels create poor perfusion and uneven drug distribution. Prolonged antiangiogenic therapy may also select coordinated downregulation of angiostatic factors in endothelial and tumor cells, producing adaptive resistance [23], whereas vascular normalization can improve oxygenation and radiosensitivity [24]. Vascular interventions should be assessed through functional perfusion, immune-cell entry, and drug distribution alongside vessel density.

Metabolic activity and ECM organization interact within organ-specific niches. Metabolic signatures associated with stromal abundance in gastric cancer provide a comparative example [25]. In lung cancer bone metastasis, SLC2A3-associated lactate metabolism, p53 lactylation, and immune escape provide a more direct anchor for organ-specific metabolic selection [26]. A network linking POSTN-positive CAFs with ACKR1-positive endothelial cells in tyrosine kinase inhibitor (TKI)-resistant lung cancer, spatial dedifferentiation in aggressive lung adenocarcinoma, and NR2F2-associated immune remodeling within CAFs all indicate that resistance and malignant progression arise from both cancer-cell transcriptional states and the spatial organization of neighboring cells [27-29]. BMP2/4-ACVR1-dependent macrophage polarization further suggests that tumor-promoting myeloid states can participate in ecosystem reorganization from tumor initiation [30], while paired spatial transcriptomes of primary tumors and brain metastases show that lesions from the same patient can develop distinct immune-defense architectures [31].

High-altitude populations adapt to sustained hypoxia through coordinated respiratory, hematologic, and metabolic regulation [32]. Tumor hypoxia is jointly shaped by cancer cells and their microenvironment and profoundly alters treatment response [33]. Natural ecology, physiological adaptation, and human migration offer three analytical coordinates for lung cancer: system boundaries, dispersal filters, and sustaining feedback. Table 1 aligns seven system transitions with their mechanistic anchors, evidence sources, domains of application, and testable propositions.

## 2. Chronic disturbance, injury-mediated selection, and lung cancer initiation

### 2.1 How homeostatic tissue becomes a selective environment

In healthy alveoli, alveolar type 1 (AT1) and type 2 (AT2) cells perform distinct functions, while an intact epithelial-basement-membrane barrier, compliant matrix, resident immune surveillance, and stable

microcirculation maintain tissue homeostasis. Chronic exposure to tobacco smoke, particulate pollution, infection, or fibrotic injury repeatedly activates epithelial repair, sustains myeloid inflammation, and alters tissue mechanics. In studies of air-pollution-associated lung adenocarcinoma, particulate matter induced macrophage-derived interleukin-1β (IL-1β) signaling and expanded pre-existing EGFR-mutant cells [34]. These findings demonstrate environmental filtering of a pre-existing clonal population.

Injury initiates repair while opening several possible trajectories. Persistent damage-associated transient progenitors (DATPs) mark stalled or delayed repair in models of alveolar injury [35]. Inflammatory memory can durably alter cellular plasticity in pancreatic models, although direct evidence in the lung remains limited [36]. In lung adenocarcinoma, matrix stiffness regulates proliferation and programmed death-ligand 1 (PD-L1) expression through YAP signaling [37]. Together, these studies identify repair arrest, cellular memory, and mechanical remodeling as parallel, context-dependent responses to tissue injury.

Loss of homeostasis begins with the failure of negative feedback. Under normal conditions, contact inhibition, basement-membrane architecture, local growth factors, and immune clearance constrain AT2-cell proliferation, and transitional cells return to mature differentiation after repair. Recurrent injury prolongs this repair window, allowing inflammatory signals, mechanical stress, and replicative stress to persist within the same tissue compartment. A driver mutation then acquires a different meaning: it is no longer constrained within a fully functional alveolar niche but operates in an abnormal habitat with fewer competitors, altered resource flow, and fluctuating immune surveillance.

Clones carrying cancer-associated variants can be detected in normal or aging tissues, yet only a fraction progress to malignancy. Niche state governs the penetrance of a mutation: the same genetic alteration may remain quiescent in homeostatic tissue but gain an expansion window during inflammation and failed repair. The growth response of pre-existing EGFR-mutant cells to particulate pollution is a direct example [34]. Studies of initiation should relate clonal changes to the history of tissue injury and repair, as well as to newly acquired mutations.

**Table 1.** Seven system transitions in lung cancer ecological evolution: mechanisms, evidence, and testable propositions

| Stage | Ecological lens | Transition in lung cancer | Mechanistic anchors | Evidence base | Scope and evidence boundary | Testable proposition |
|---|---|---|---|---|---|---|
| I System assembly | Ecosystem; niche construction | Cancer, immune, stromal, and vascular cells assemble with oxygen, pH, ECM, and drug gradients | TAMs; MDSCs; Tregs; CAF-TGF-β/CXCL12; abnormal vessels | Human lung atlases; single-cell and spatial studies [6, 10, 11] | Open; host-dependent | The microenvironment is a measurable, targetable system component |
| II Disturbance and initiation | Environmental filtering; competitive release | Chronic injury weakens normal epithelium and opens an expansion window for abnormal clones | DATPs; ROS/RNS; YAP-TAZ; APOBEC; WGD | Pollution and injury models; TRACERx [34-38] | Parallel mechanisms; tissue-dependent | Genetic change and damaged habitat jointly drive lung cancer initiation |
| III Local takeover | Reciprocal adaptation; immune selection | Myeloid recruitment and immune-state remodeling extend suppression from local tissue to the host | CCL2-CCR2; TREM2; TOX-NR4A; PD-L1-positive EVs; metabolic competition | Spatial, functional, and epigenetic studies [39-45] | Cancer cells: mainly genetic change; host cells: mainly state remodeling | Immunotherapy should be evaluated at the tumor-immune-system level |
| IV Boundary advance | Ecotone; selective gate | Directed tumor invasion occurs as immune entry is restricted | FAK/LOX-ECM; CXCL12-CXCR4; MCT4-lactate; MMP-9/14 | Lung cancer spatial and pathologic studies [10, 11, 46, 47]; metabolic and matrix mechanisms [48-52] | Functional correspondence: selective permeability | The invasive front links tumor-cell egress to immune exclusion |
| V Cross-habitat dissemination | Selective bottleneck; founder effect | Rare subclones leave the thorax, survive circulation, and seed distant organs | SCNAs/CIN; CTC clusters; platelets/neutrophils; EV organotropism | Human lung cancer cohorts; cross-cancer mechanisms [53-59] | Emigrants are a non-random clonal subset; organ niches impose further selection | A single metastasis represents only part of the patient-wide lineage structure |
| VI Network formation | Metapopulation; source-sink switching | Intermetastatic reseeding converts recipient lesions into secondary sources | Organ filtering; local reprogramming; secondary output | Multiregion and autopsy sequencing; cross-cancer network studies [53, 60-62] | Human evidence is mainly longitudinal and phylogenetic; lesion roles change with treatment | Local treatment should account for lesion output and network effects |
| VII Treatment selection | Directional selection; competitive release; refugia | Sensitive populations contract as DTPs and resistant clones survive and rebuild the relapse ecosystem | Pharmacokinetic, anatomical, and physiological refugia; APOBEC3A; TGF-β2; lineage switching | Mechanistic studies, case reports, and pilot trials [63-68] | Limited prospective validation in lung cancer | Treatment should integrate killing, competition, and the cost of escape |

Abbreviations: CAF, cancer-associated fibroblast; CIN, chromosomal instability; CTC, circulating tumor cell; DATP, damage-associated transient progenitor; DTP, drug-tolerant persister; ECM, extracellular matrix; EV, extracellular vesicle; MDSC, myeloid-derived suppressor cell; RNS, reactive nitrogen species; ROS, reactive oxygen species; SCNA, somatic copy-number alteration; TAM, tumor-associated macrophage; Treg, regulatory T cell; WGD, whole-genome doubling.

Chronic injury impairs the survival and repair capacity of normal epithelium, giving abnormal clones a relative advantage, whereas cells that lack an adaptive survival advantage die or become senescent. Cell-death programs that release or expose defined damage-associated molecular patterns and activate adaptive immunity constitute immunogenic cell death [69]; senescent cells release senescence-associated secretory phenotype (SASP) factors [70]. These outcomes alter local antigen exposure and inflammatory signaling and drive ECM remodeling. As normal epithelial-cell number and function decline, clones previously constrained by space and resources gain room to expand even without an increase in their intrinsic proliferation rate. Chronic inflammation both damages tissue and lights the fuse for expansion of pre-existing abnormal clones.

## 2.2 Pioneer clones and niche construction

Multiregion analyses from TRACERx (Tracking Cancer Evolution through Therapy) have resolved the complex timing of subclonal selection, copy-number change, and whole-genome doubling in lung cancer [38]. Spatial multi-omics of precursor lesions has further identified alveolar progenitors with tumor-associated programs colocated with proinflammatory niches, supporting reciprocal remodeling between abnormal epithelium and local inflammation before invasive cancer develops [71]. Intravital lineage tracing shows that lung adenocarcinoma cells can lose a stable AT2 identity, pass through a transient state of high plasticity, and enter divergent evolutionary trajectories [72].

We define the earliest abnormal populations that breach homeostatic constraints and remodel their surroundings as "pioneer clones." Their identity is ecological rather than tied to a fixed molecular lineage. Hypoxic and metabolic adaptation, paracrine signaling, early vascular recruitment, and immune exclusion can give these clones an expansion advantage; evidence for lactate-based metabolic symbiosis remains stronger in models than in direct measurements of human tumor flux [73]. An early expanding clone may later disappear after altering stromal and immune conditions for other clones, while a small clone may expand rapidly after vascular access, altered immune pressure, or local release from spatial constraints. Temporal and spatial sampling of precursor lesions can reveal niche-modifying populations that disappear before endpoint sampling.

Abnormal clones construct niches along three main axes: resources, immune risk, and tissue space. Resource acquisition includes enhanced glycolysis, lactate use, angiogenesis, and amino-acid competition. Immune-risk reduction includes impaired antigen presentation, exclusion of cytotoxic lymphocytes, and recruitment of suppressive myeloid cells. Spatial remodeling includes collagen deposition and alignment, basement-membrane remodeling, and the formation of migration channels. These axes can advance together in combinations that vary by lung cancer subtype and stage.

Immune clearance further shapes clonal composition. Patient-derived organoid-T-cell cocultures reveal different escape capacities among non-small cell lung cancer (NSCLC) subclones [74], while TRACERx identified human leukocyte antigen (HLA) loss of heterozygosity, neoantigen copy-number loss, and transcriptional silencing as routes of immune evasion [75]. Immune pressure therefore enriches subclones with antigen loss or defective presentation. Fig. 1 links healthy homeostasis, chronic disturbance, pioneer clones, and invasion as a transfer of tissue control: repair, barrier integrity, and surveillance recede as resource redirection and suppressive immunity rise.

## 2.3 Repair memory, field effects, and the premalignant niche

Studies of lung cancer initiation must look beyond the two endpoints of "normal lung" and "tumor." Smoking, pollution, chronic infection, and fibrosis can remodel broad regions of lung tissue before a malignant lesion becomes detectable, creating spatially continuous field effects. Imaging of healthy, fibrotic, and emphysematous ECM in precision-cut human lung slices has quantified structural reorganization of collagen and elastic fibers [76]. These changes are not themselves premalignant lesions, but they redefine the boundaries of adhesion, migration, and mechanosensing, allowing clones with the same driver event to follow different trajectories in different tissue regions.

Repair also leaves a memory in cellular composition. Restoration of homeostasis after viral lung injury requires coordinated epithelial repair and timely resolution of innate immunity [77]. Studies of alveolar epithelial stem cells and their niches show that the temporal coordination of AT2 cells, transitional progenitors, fibroblasts, and immune cells determines whether repair finishes on schedule or proceeds to pathological remodeling [78].

Recurrent injury creates patchy field effects with unequal inflammatory intensity, matrix structure, and clonal composition. Some regions retain an intact barrier and immune surveillance; others accumulate stiff matrix, abnormal vessels, and persistent myeloid inflammation. A pioneer clone in the latter environment encounters weaker competition and a longer repair window, gaining an opportunity for

expansion without an increase in its intrinsic malignant potential. This relationship helps explain why similar exposures and driver events lead to different outcomes. Premalignant cohorts should link clonal lineages to repair history, ECM architecture, and immune organization through measurements within the same tissue regions.

The premalignant niche also determines the scale of early intervention. Removing an imaging-visible lesion may leave surrounding tissue that continues to select abnormal clones, whereas broadly suppressing inflammation or matrix deposition may disrupt essential repair. Productive targets are local feedbacks that fail to restore homeostasis, including persistent DATP-like states, prolonged IL-1 signaling [34, 35], abnormal collagen alignment, and immune exclusion. Longitudinal studies should track persistent repair states, inflammatory signaling, and tissue architecture. Intervention studies can then test whether reversing these abnormalities reduces abnormal-clone expansion.

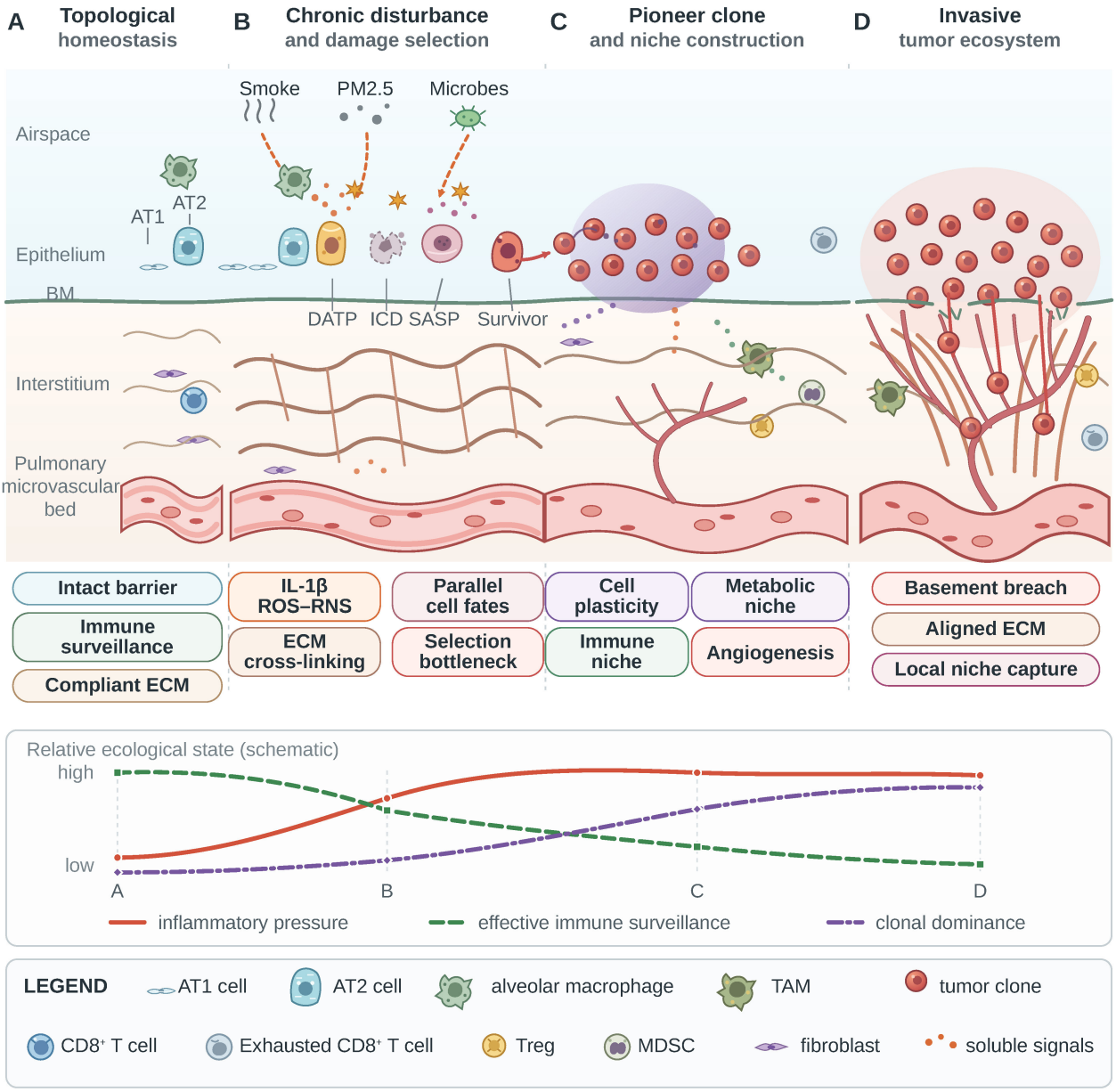



**Figure 1.** Ecological emergence of invasive lung cancer. (A) Healthy alveolar tissue maintains topological homeostasis through ordered alveolar type 1 (AT1) and type 2 (AT2) epithelial cells, an intact epithelium-basement membrane (BM), compliant extracellular matrix (ECM), resident immune surveillance, and an organized pulmonary microvascular bed. (B) Recurrent exposure to smoke, PM2.5, and microbial disturbance activates inflammatory signaling, reactive oxygen and nitrogen species (ROS/RNS), maladaptive epithelial repair, and ECM cross-linking. Damaged epithelial cells enter damage-associated transient progenitor (DATP), immunogenic cell death (ICD), senescence-associated secretory phenotype (SASP), or rare-survivor states as parallel, context-dependent outcomes. (C) Selected survivors acquire plasticity and expand as pioneer clones, while hypoxic-metabolic adaptation, tumor-associated macrophages (TAMs), myeloid-derived suppressor cells (MDSCs), regulatory T cells (Tregs), pale blue exhausted CD8+ T cells, and proangiogenic signaling construct an immune-vascular niche. (D) Continued tumor-microenvironment co-evolution produces BM breach, aligned ECM tracks, invasion, and a denser tumor-associated vasculature, establishing a locally dominant ecosystem. The lower trajectories schematically show increasing inflammation and clonal dominance with declining effective immune surveillance across a conceptual ecological continuum.

## 3. Coordinated remodeling by tumor, immunity, and stroma

### 3.1 Rewriting the local immune niche

Models of early NSCLC show that tissue-resident macrophages can establish a tumor-promoting niche for abnormal epithelium [39]. In lung squamous cell carcinoma, CAF-derived CCL2 recruits CCR2-positive monocytes and promotes their differentiation into suppressive MDSCs [79]. Pan-cancer single-cell studies have identified a TREM2-associated immunosuppressive program, although its origin and prevalence among lung-resident macrophages remain unresolved [40]. Persistent antigen exposure and metabolic stress can also stabilize $CD8^+$ T-cell exhaustion through TOX, TOX2, and NR4A networks [41]. Myeloid recruitment, functional reprogramming, and T-cell exhaustion together allow the tumor to co-opt host immunity and progressively create an immune state favorable to its persistence.

Immune co-option spans distinct cell lineages and differentiation states. Alveolar-resident macrophages, monocyte-derived macrophages, and tissue macrophages in metastatic organs have different developmental origins and modes of replenishment. Early lesions can exploit resident repair programs, whereas advanced tumors intensify peripheral myeloid recruitment. A binary M1/M2 classification and individual markers such as CD163 or TREM2 cannot capture this heterogeneity; tumor-associated macrophages (TAMs) must be defined by lineage, spatial proximity, and function. T-cell exhaustion likewise develops along a continuum. Progenitor exhausted cells may still respond to treatment, whereas terminal exhaustion is constrained by more stable chromatin programs. Evaluation of $CD8^+$ T cells should integrate abundance, location, differentiation state, contact with target cells, and functional reversibility.

The pulmonary microbiota can also reshape local immunity over time. In mice, lung commensals activate γδ T cells and IL-17-associated inflammation to promote lung cancer [80]. In patients, dysbiosis of the lower-airway microbiota has been associated with disease progression and stronger IL-17 and PI3K-MAPK-ERK signaling [81].

Diffusible signals extend immunosuppression beyond the local lesion. In experimental models, exosomal PD-L1 mediates systemic immune suppression, and blocking its release enhances antitumor immunity [42, 43]. In an NSCLC cohort, circulating exosomal PD-L1 was associated with disease control and progression-free survival [82]. Metabolic competition weakens immunity through another route: SLC43A2-dependent methionine uptake reduces methionine available to T cells and alters histone methylation [44], providing a direct mechanism for tumor "resource capture".

Local and systemic immunosuppression are coupled through the circulation. Extracellular vesicles (EVs) and cytokines released by the primary lesion enter the bloodstream; altered myelopoiesis in bone marrow and immune tolerance in lymph nodes then feed back on local infiltration. The primary tumor can reset the host immune baseline before cancer cells reach distant organs, creating conditions that favor dissemination.

The effect of interferon-γ (IFN-γ) depends on tissue context, timing, and the responding cell. During skeletal-muscle repair, regulatory T cells (Tregs) regulate macrophage accumulation and phenotype by limiting IFN-γ [83]. In tumor models, IFN-γ can instead induce Treg fragility and strengthen antitumor immunity [84]. Applying pan-cancer immune archetypes to lung cancer requires assessment of their spatial distribution within individual lesions [85].

Hypoxia can reshape both cancer cells and the immune microenvironment through RNA processing. In NSCLC, hypoxia-associated alternative polyadenylation of CARM1 has been linked to microenvironmental change [86]. Tumor-infiltrating clonal hematopoiesis further complicates the origin of myeloid signals because some variants detected within a lesion arise from host hematopoietic clones [87]. Matched sequencing of peripheral-blood hematopoietic cells helps distinguish hematopoietic-clone variants from tumor-derived variants in liquid-biopsy and single-cell analyses.

### 3.2 Plasticity, persistence, and dormancy

Tumor stemness is a dynamic state that cells can enter and leave. In EGFR-mutant lung cancer, chromatin remodeling supports the reversible drug-tolerant persister (DTP) state [45]. DTPs in colorectal cancer models adopt a diapause-like state characterized by low MYC activity and reduced protein synthesis [88], surviving by lowering growth and biosynthetic demand.

Plasticity allows tumor cells to respond to treatment through state transitions in addition to genetic variation. Selection of pre-existing variants and reversible state change jointly drive resistance: resistant clones expand directly, whereas the DTP state prolongs survival and creates time for subsequent mutation and reprogramming. A pretreatment specimen therefore has an inherent ceiling in its ability to predict the path of resistance.

Dormancy and reawakening are jointly controlled by cell-intrinsic programs and the local

habitat. In mouse lungs, inflammation-induced neutrophil extracellular traps (NETs) awakened dormant breast cancer cells through basement-membrane remodeling [89]. In mammary and head-and-neck tumor systems, a tumor-derived type III collagen-rich matrix maintained dormancy through DDR1-STAT1 signaling [90]. Inflammation and matrix remodeling after infection, injury, or treatment can disrupt the equilibrium that holds residual cells dormant and permit renewed proliferation.

Dormant cells retain metabolic and stress-response activity, and micrometastases may persist through a long-term balance between slow proliferation and cell death. Absence of a radiologically detectable lesion may reflect eradication, persistent dormancy, or indolent growth. Circulating tumor DNA (ctDNA) can improve detection of minimal residual disease, but a negative result remains constrained by DNA shedding and assay sensitivity [91].

## 4. The invasive-front ecotone and its selective gates

### 4.1 Mangrove ecotones and asymmetric penetration

Mangroves occupy the convergence of riverine freshwater, tidal saline water, and hypoxic sediment. Distinct plant communities and root architectures support aeration, sediment retention, and wave attenuation, while shifting with tides and seasons. The lung cancer invasive front likewise brings together tumor cells, CAFs, myeloid cells, lymphocytes, vasculature, and continuously remodeled ECM. Both systems lie between opposing flows of matter and cells, and their boundary architecture determines what can cross and how efficiently.

Mangroves absorb waves moving from sea to land while receiving river flow and nutrients moving toward the sea. At the invasive front of lung cancer, tumor cells expand into normal lung as host immune cells attempt to penetrate the tumor. Aligned collagen fibers, abnormal vessels, and tissue spaces can provide outward routes for cancer cells, whereas dense matrix, distorted chemokine gradients, and bands of suppressive myeloid cells impede entry by $CD8^+$ T cells and natural killer (NK) cells. The same boundary therefore imposes different resistance in opposite directions and functions like a "one-way valve".

Fig. 2 frames this asymmetry as a spatial structure. Overlapping functional zones regulate cross-boundary flow in the mangrove ecotone, while cellular, biochemical, and physical barriers at the lung cancer invasive front separate the routes of cancer-cell egress from those of effector-lymphocyte entry. Opposing paths with unequal penetration depths show that boundary behavior depends on both the migrating entity and its direction and cannot be summarized by a single measure of barrier strength.

Tumor-reactive T cells in peripheral blood do not ensure effective killing within the tumor. T cells must arrive, penetrate, recognize their targets, and sustain effector function. Failure at any step limits killing; impaired penetration creates an immune-present but contact-poor state. Neither PD-L1 expression nor total T-cell density alone captures this spatial checkpoint. At this ecological frontline, cancer-cell egress and immune exclusion are coupled within the same spatial unit.

### 4.2 Composite barriers and focal breach

The invasive barrier emerges from the spatial combination of cells, signals, and matrix. In a KRAS/LKB1-comutant lung adenocarcinoma model, FAK-activated CAFs promoted collagen deposition and formed a physical barrier to $CD8^+$ T-cell infiltration. FAK inhibition reduced collagen, increased entry of effector immune cells, and enhanced programmed cell death protein 1 (PD-1) blockade [46]. In small-cell lung cancer, the CXCL12-CXCR4 axis recruits $CXCR4^+$ neutrophils and $S100A8^+$ monocytes to the tumor-normal interface, where they become spatially segregated from $CD8^+$ T cells [10]. Spatial analysis of lung cancer further shows that the pattern of adjacency between $CD163^+$ macrophages and lymphocytes influences immune escape and clinical outcome [11].

Basement-membrane continuity, collagen density and orientation, pore size, and interstitial pressure create the physical barrier. pH gradients, chemokine fields, and matrix-degrading activity form the biochemical barrier, while the relative positions of CAFs, myeloid cells, and effector lymphocytes create the cellular gate. These layers reinforce one another: matrix stiffening changes migration and signaling, myeloid factors activate CAFs and remodel ECM, and hypoxia and acidosis weaken immune function. Compensation across layers limits the effect of a single-point intervention.

Tumors commonly break through at a small number of sites along the front. Tumor budding, perivascular migration, spread through air spaces (STAS), and extension along pre-existing tissue planes may coexist, with focal gaps interrupting an otherwise continuous basement membrane. Fig. 2 connects such localized escape routes to the surrounding composite barrier. TRACERx has linked lung adenocarcinoma histologic patterns to distinct subclonal somatic copy-number alterations (SCNAs), recent clonal expansions, and recurrence routes [47]. Histology therefore records

how clones occupy space and disseminate outward. A regional specimen that misses a rare breach can underestimate the invasive capacity of the lesion.

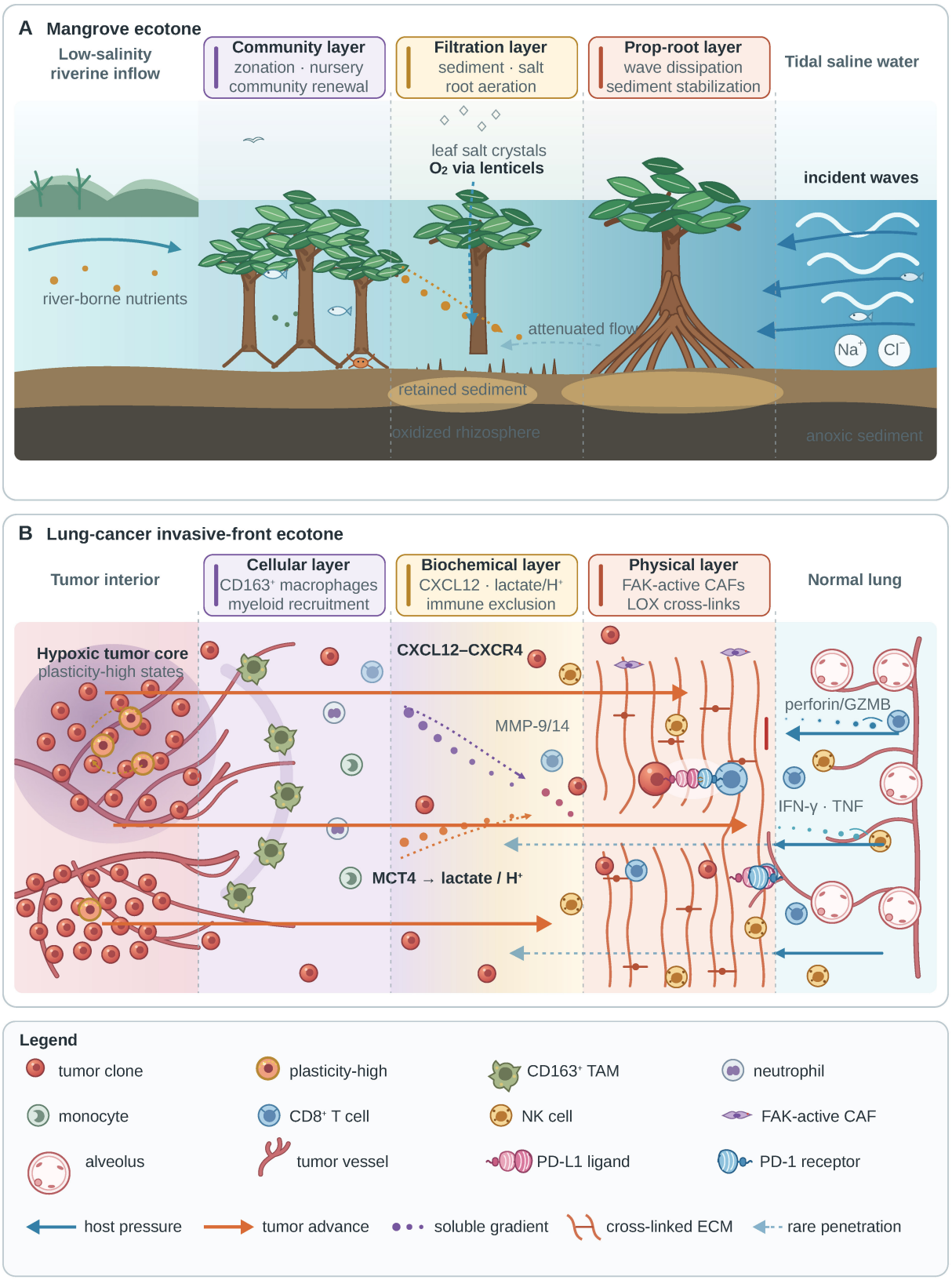



**Figure 2.** Mangrove and lung cancer invasive-front ecotones. (A) A conceptual mangrove transect extends from low-salinity riverine inflow to tidal saline water. The community zone represents vegetation zonation, nursery habitat, and renewal; the filtration zone represents sediment retention, salt regulation, and root aeration; and the seaward prop-root zone represents sediment stabilization and dissipation of wave energy. Pale halos denote the oxygenated rhizosphere around aerating roots, and the deeper dark layer denotes anoxic sediment. These overlapping ecological functions shift across the transect. (B) The lung cancer invasive front is a selectively permeable ecotone between a hypoxic, heterogeneous tumor and ordered normal lung. Irregular vessels and highly plastic clones occupy the tumor side. A discontinuous band of CD163+ tumor-associated

macrophages (TAMs), together with neutrophils and monocytes, forms a cellular gate; CXCL12-CXCR4 signaling, MCT4-associated lactate and proton export, and MMP-9/14-mediated matrix degradation form a biochemical gate; and FAK-active cancer-associated fibroblasts (CAFs), LOX-dependent collagen cross-linking, and dense ECM form a physical gate. Orange routes show tumor advance to unequal depths, whereas blue routes show heterogeneous penetration by host immunity. CD8+ T cells and natural killer (NK) cells impose perforin, granzyme B (GZMB), IFN-γ, and TNF pressure, while tumor-cell PD-L1 engages PD-1 on CD8+ T cells. Ordered host microvessels and alveoli contrast with the tortuous tumor territory. The three tumor-front zones correspond to mangrove zones through shared boundary functions.

Metabolites are both resources and modifiers of the boundary environment. Human isotope tracing shows that NSCLC can take up circulating lactate and feed it into the tricarboxylic acid cycle [48]. In LKB1-deficient lung adenocarcinoma, MCT4-dependent lactate secretion promotes suppressive macrophage polarization and impairs T-cell function [49]. The ZEB1-LOXL2 axis increases matrix stiffness through collagen deposition and cross-linking [50], whereas MMP-9 and MMP-14 open migratory routes through matrix degradation [51, 52]. Lactate secretion, collagen cross-linking, and matrix degradation together alter acidity, mechanics, pore structure, and immune accessibility at the invasive front.

Dense collagen forms a "physical trench," while suppressive myeloid bands provide an immune "umbrella." Their strength can be assessed through collagen density, chemokines, immune penetration, and perfusion. Barrier-directed interventions may improve drug and immune-cell entry while also easing cancer-cell escape. Evaluation should pair intratumoral drug distribution and immune penetration with measures of tumor-cell dissemination.

### 4.3 Dynamic boundaries and windows of dissemination

The invasive front advances, pauses, and changes direction as cells die or proliferate and as vascular access and ECM architecture are remodeled. Studies in breast cancer place anoikis, necroptosis, and ferroptosis among the selective processes at metastatic fronts [92]. Reactive oxygen species (ROS) can kill circulating cells, whereas sublethal ROS can promote migration and stress adaptation [93]. Cell death clears susceptible populations, while rare stress-tolerant survivors gain opportunities to expand as conditions at the front change.

Neutrophils and MDSCs add a temporal rhythm to the boundary. Neutrophil recruitment, NET formation, and antitumor activity vary with disease stage and cell state [94], while MDSCs can sustain immunosuppression in residual and recurrent disease [95]. A single-time-point map of the invasive front will miss transient barrier opening and rapid reconstruction. Serial biopsy is rarely feasible in lung cancer, making it more practical to align spatial pathology with longitudinal blood measurements, imaging, and treatment events and to identify surrogate markers of barrier opening and reformation.

Whether cancer cells cross the boundary and enter the circulation as single cells or clusters affects their survival and metastatic efficiency. Circulating tumor cell (CTC) clusters retain cell-cell adhesion and may carry immune or stromal cells as heterotypic aggregates; they generally survive circulation and seed metastases more efficiently than individual CTCs [96]. CTC analysis can profile populations currently disseminating, but enrichment methods, dependence on epithelial markers, and low abundance introduce sampling bias [97]. CTCs alone rarely identify the lesion of origin or final destination.

The invasive front also exports signals to distant organs through extracellular vesicles. EV communication between lung cancer cells and their microenvironment contributes to premetastatic niche formation [98]. Vesicles from different sources mix in the circulation, so their organ directionality and effective dose cannot be reconstructed from a clinical blood sample alone. Disseminated cancer cells subsequently face organ-specific selection and may enter dormancy, processes that continue to shape metastatic outcome [99]. At this ecological frontline, local selection shapes the cells and signals entering the systemic circulation.

## 5. Serial bottlenecks and distant founding during cross-compartment dissemination

### 5.1 "Out of Africa" and serial founder effects

Modern human origins in Africa are best represented by a pan-African history in which multiple structured populations interacted and gradually converged [100, 101]. Several early dispersals left little ancestry in present-day populations outside Africa, whereas the successful expansion approximately 50,000-60,000 years ago passed through a founder bottleneck and produced a decline in genetic diversity with distance from the source [102, 103]. Dispersing populations also underwent limited introgression with Neanderthal- and Denisovan-related groups; EPAS1-mediated high-altitude adaptation is a classic example of adaptive introgression [104, 105].

Migration continued to reshape regional populations after initial settlement. Ancient genomes record large-scale migration and replacement in Europe by Bronze Age steppe populations [106], showing how repeated expansion, mixing, and

replacement can unfold over successive periods. Fig. 3A condenses human dispersal into structured African source populations, founder bottlenecks, and regional expansion, with paternal-lineage frequencies changing through serial sampling. Human populations undergo sexual recombination and archaic introgression, whereas tumors expand clonally; the shared structure lies in non-random emigration, founder effects, and serial bottlenecks. In lung cancer, subclones disseminating at different times encounter successive bottlenecks and may contribute unequally to distant lesions.

Serial founder effects expose a fundamental limitation of endpoint sampling: the small number of individuals leaving a source population cannot carry all of its diversity. Metastatic diversity does not decline monotonically with anatomical distance, and polyclonal colonization can reintroduce local heterogeneity. Even so, a single metastasis records only the lineages that successfully dispersed and survived. Reconstructing the primary clonal pool from an endpoint lesion will therefore underestimate subclones that disappeared or never emigrated.

### 5.2 Non-random emigration and cross-compartment selection

The joint TRACERx-PEACE (Posthumous Evaluation of Advanced Cancer Environment) study enrolled 24 patients with NSCLC and deeply sequenced 501 primary and metastatic samples collected at surgery, recurrence, and autopsy. Tissue was obtained for approximately 70% of all metastases detected radiologically before death [53]. In 62.5% of patients, different primary subclones independently founded separate metastases, and more than half of sampled metastases were themselves seeded by another metastasis. Most migration occurred within the same anatomical compartment. The smaller group of subclones that left the thorax spread more widely and was enriched for somatic copy-number alterations. Because 88% of the cohort received systemic therapy, these proportions require validation in untreated disease and in patients presenting with *de novo* metastasis.

Chromosomal instability can promote metastasis through cytosolic DNA sensing, providing a mechanistic basis for enrichment of SCNAs [54]. SCNA enrichment may contribute to fitness during cross-compartment spread. Prospective testing in diagnostic specimens is needed to establish its predictive value. Successful emigrants are a non-random sample of the primary clonal pool, and an individual metastasis retains only a fraction of the lineages that disseminated successfully. ctDNA combines signals from several lesions, with their contributions weighted by volume, perfusion, anatomical site, and DNA shedding [107]. This variable weighting limits reconstruction of the patient-wide clonal composition.

Intrathoracic migration and extrathoracic dissemination face different selection thresholds. Movement among lung, pleura, and mediastinal lymph nodes occurs within related anatomical and circulatory contexts. Entry into brain, liver, or bone requires successive passage through the bloodstream, endothelial barriers, and organ-specific niches. Intrathoracic and extrathoracic routes therefore require separate mechanistic analysis. If SCNAs or chromosomal instability increase the capacity for extrathoracic spread, their clinical value will depend on recognizing high-risk clones before metastasis occurs.

Founder number further determines the initial composition of a metastasis. Monoclonal founding produces a narrow genetic spectrum, whereas polyclonal founding establishes a broader genetic and phenotypic range from the outset and increases the chance that a single target will leave an uncovered subpopulation. Detecting polyclonal dissemination requires adequate sequencing depth and multiregion sampling; low tumor purity and limited sampling systematically underestimate its frequency.

### 5.3 Lymph-node relay and selection in the circulation

Fig. 3B follows lung cancer from intrathoracic expansion into the circulatory bottleneck. Mouse models show that lymph-node metastases can enter local blood vessels and disseminate further [55], and that colonization of lymph nodes can induce Treg-dependent immune tolerance [56]. In TRACERx, however, lymph-node metastases sampled at resection seeded less than 20% of subsequent recurrences or progressive lesions [60]. These findings support lymph-node involvement in selected dissemination routes, through both vascular access and immune regulation.

Tumor cells entering the bloodstream face stringent selection by shear stress, loss of anchorage, oxidative stress, and NK-cell attack. NKG2D-dependent mechanosensing links shear forces to NK-cell killing [57]. Platelet coating, neutrophil association, and clustering increase the survival of selected cells. Direct evidence that CTC clusters have greater colonizing capacity and oligoclonal origins comes largely from breast cancer [58]; clustering can also reshape DNA methylation and strengthen stemness-associated programs [108]. Fig. 3B therefore depicts the circulation as a sequence of entry, attrition, and rare survival.

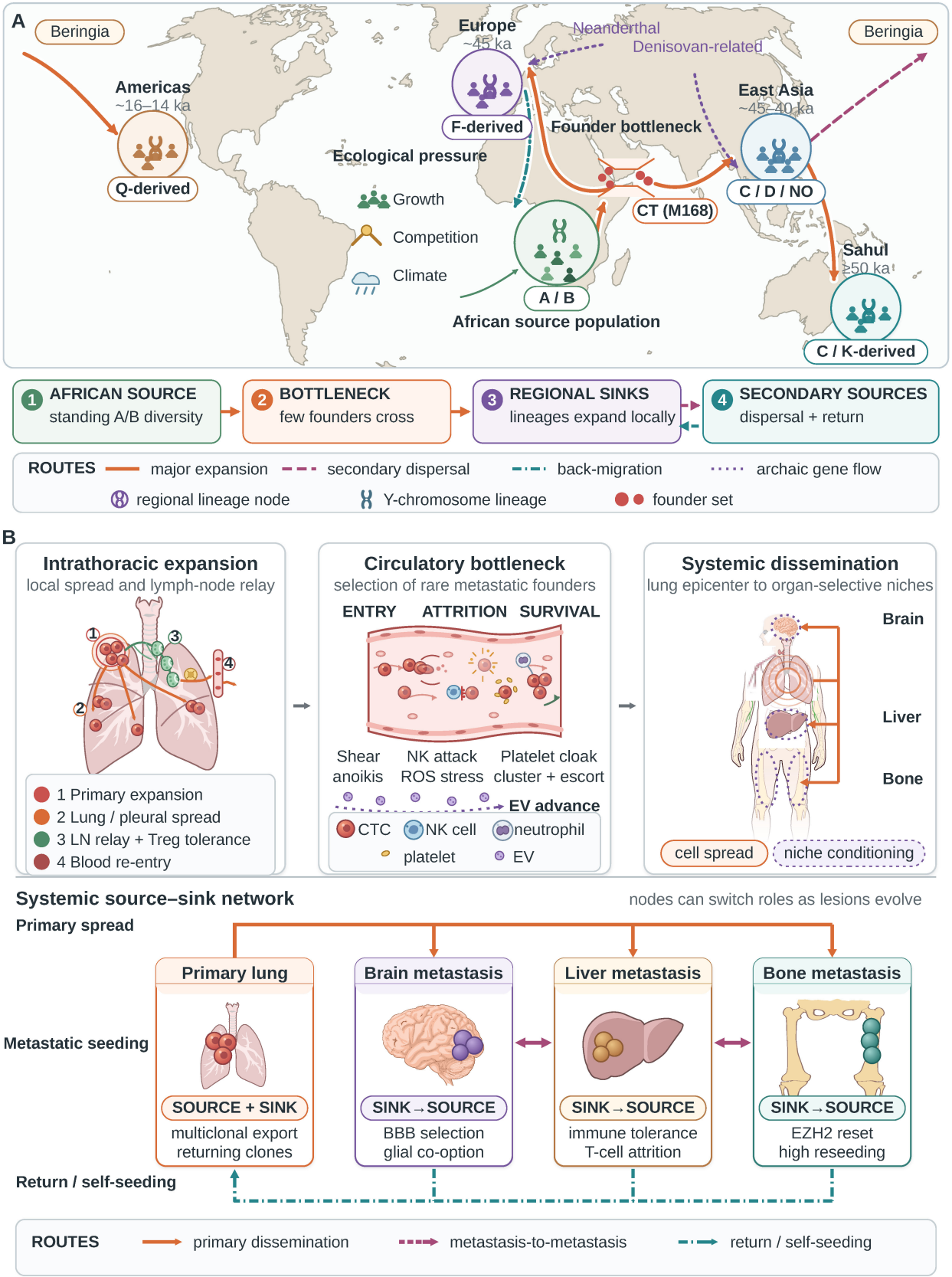



**Figure 3.** Ecological dispersal as an analogy for lung cancer source-sink dynamics. (A) Structured African populations form the initial source, where demographic growth, resource competition, and climate variability create ecological pressure. A founder bottleneck precedes expansion into regional sinks, followed by lineage enrichment, secondary dispersal, return migration, and archaic gene flow. Solid orange routes show major expansion, dashed magenta routes show secondary dispersal, teal dash-dot routes show return migration, and dotted violet routes show archaic gene flow. A, B, CT, C, D, NO, F, K, and Q denote simplified Y-chromosome paternal lineages and broad phylogeographic enrichment (used here as an abstract analogy for clonal bottlenecks and changes in lineage frequency). (B) The primary lung tumor expands through intrapulmonary and pleural spread and a lymph-node relay that supports immune tolerance and re-entry into blood. Circulating tumor cells face shear stress, anoikis, NK-cell attack, and oxidative stress, while platelet coating, neutrophil association, and clustering may protect rare metastatic founders. Extracellular vesicles (EVs) can condition organ-

selective niches before tumor-cell arrival. In the source-sink network, the primary lesion both exports and receives cells; metastases become secondary sources, seed one another, and may return to or self-seed established lesions. Brain, liver, and bone represent organ-dependent selection and reprogramming. Human NSCLC phylogenies support intermetastatic reseeding, whereas experimental self-seeding models provide the return-flow route. Anatomical artwork was adapted from the NIAID NIH BioArt Source (public domain).

Circulatory selection reshapes the composition of the disseminating tumor-cell population. A clone that dominates the primary lesion may be cleared in circulation, while a rare state may be enriched through resistance to anoikis, antioxidant capacity, or collective protection. Platelets and neutrophils can protect CTCs and, in other inflammatory states, participate in their clearance. Their net effect depends on the mode of interaction and disease stage. Traits favored during local expansion may differ from those required for circulatory survival and distant colonization.

### 5.4 Distant-organ entry, dormancy, and initial colonization

After surviving circulation, tumor cells must cross the endothelium and adapt to the vascular architecture, ECM, resident immunity, and nutrient conditions of a distant organ. In a murine breast cancer model, hypoxia-induced integrin β3-positive extracellular vesicles promote brain metastasis [59]. In Lewis lung carcinoma and melanoma models, vascular endothelial growth factor receptor 1-positive (VEGFR1+) bone-marrow-derived progenitors accumulated in distant tissue before cancer-cell arrival and helped establish a premetastatic niche [109]. These advance signals remodel the local environment and change the entry threshold of the distant organ.

Colonization requires survival beyond initial organ entry. Most disseminated cells are cleared; a minority become dormant or establish micrometastatic communities. ECM composition and remodeling regulate dormancy and reawakening in experimental breast cancer and head-and-neck tumor systems [89, 90]. Local immune activity contributes to the clearance or persistence of residual cells and influences their return to growth [110]. Successful founding requires long-term survival and the formation of sustaining interactions with local cells and matrix.

Dormant residual cells can persist despite the absence of detectable disease. Interventions can either eliminate residual cells as seeds of recurrence or maintain quiescence to prevent reawakening [111, 112]. Liquid biopsy detects tumor signals released by some forms of minimal residual disease, but slowly proliferating, poorly shedding dormant cells may remain below the detection threshold [91]. Longitudinal imaging and molecular surveillance are needed to assess residual disease in distant organs because a single negative result may reflect levels below the detection threshold.

Fig. 3B connects premetastatic conditioning to organ entry and selection in the brain, liver, and bone. Advance signaling adds a distinct feature to the migration analogy: a primary tumor can influence a distant habitat before cancer cells arrive, whereas human migrants generally adapt to or remodel their destination after settlement. Local invasion, circulatory survival, organ entry, dormancy, and reawakening form a metastatic cascade in which selection intensity changes from one stage to the next [113]. Lesions that survive these bottlenecks continue to evolve, bringing lung cancer into a multi-lesion phase.

## 6. Source-sink switching and reseeding in multi-lesion evolution

### 6.1 Timing and topology of metastatic seeding

Fig. 3A shows settled regional populations becoming new centers of emigration. A metastasis founded by a few cells can likewise expand and supply founders to another organ. Fig. 3B extends this sequence into a network of lesions exchanging cells and signals.

Metastatic lineages may diverge early. Among 126 NSCLC tumors in the TRACERx cohort, metastatic divergence preceded the final clonal sweep in the primary tumor in 25% of cases; single-region sampling would have misclassified 83% of late-divergence cases as early divergence. Polyclonal dissemination occurred in 31.7% (40/126) and was associated with extrathoracic recurrence [60]. A resection specimen may therefore miss the earliest emigrant, while sparse sampling distorts timing and founder composition.

TRACERx-PEACE resolved interlesional seeding: among 258 metastases with reconstructable routes, 60% were seeded by another metastasis, 38% by the primary tumor, and 2% by both; metastases with a longer duration *in situ* were more likely to seed additional lesions [53]. Prostate-cancer genomes support metastasis-to-metastasis migration [61], and a registry-informed stochastic model of breast cancer estimates the contribution of secondary seeding [62]. An established metastasis can acquire further drivers or whole-genome doubling before exporting new founders.

Metastases form an evolving network in which several lesions can contribute to continued dissemination. A single primary region or metastasis samples only part of the lineage structure; extinct founders, unsampled lesions, and intermetastatic

migration complicate reconstruction of the complete network.

### 6.2 Source-sink switching and lesion output

Metapopulations comprise local populations linked by migration, extinction, and recolonization [114]. Demographic source populations have a local reproductive surplus; sinks depend on immigration to offset local losses [115]. Phylogenetic seeding sources identify lesions that contributed founders to another site. Fig. 3B connects this observable seeding role to the ecological question of how local growth and migration sustain the network.

Lesions export both cancer cells and signals. Cellular export supplies potential founders, while EVs and cytokines can modify immunity and distant tissue. These outputs require different measurements. Phylogenies reconstruct seeding relationships, imaging characterizes lesion burden and habitat, and ctDNA tracks tumor-derived plasma signal [107]. Comparing these observations across lesions can test how perfusion, viable burden, and clonal composition influence systemic dissemination.

A recipient lesion can expand and become a secondary seeding source. Treatment changes these contributions by suppressing some populations while allowing resistant lesions to persist. Local intervention can then be evaluated for its effects on cellular export, circulating signals, and the distribution of treatment pressure across the remaining lesions.

Response Evaluation Criteria in Solid Tumors (RECIST) summarizes lesions by diameter. Simultaneous regression, stability, and progression also reveal lesion-specific differences in genetics, habitat, and treatment sensitivity. Pairing burden measurements with seeding histories and systemic signals could identify lesions with disproportionate contributions to disease progression. Table 2 organizes the quantitative evidence and its clinical implications.

Operational definitions distinguish lesion burden, local growth, and dispersal. A cell-balance model separates local proliferation and death from emigration and successful immigration. Directed phylogenetic edges identify inferred seeding relationships, whereas cell flux requires separate quantitative estimation. A complementary occupancy matrix records transitions between absence and presence of viable populations within predefined anatomical units over an interval $\Delta t$ [114]. In clinical observations, the corresponding state records detectable disease: appearance includes occult deposits crossing the detection threshold, and disappearance can leave dormant cells. Multiple units can remain occupied simultaneously.

**Table 2.** Quantitative evidence and clinical implications of multi-lesion dissemination in lung cancer

| Network feature | Key observation | Network interpretation | Evidence base | Clinical implication |
|---|---|---|---|---|
| Multiple primary founders | 62.5% of patients had metastases founded independently by different primary subclones | Systemic disease can arise from several seeding subclones | 24 NSCLC patients; 501 samples; multiregion autopsy sequencing [53] | A single metastasis represents only part of the systemic lineage structure |
| Anatomical barriers | Most migration occurred within one anatomical compartment; fewer subclones crossed the thoracic boundary | Intrathoracic spread and distant founding face different selection pressures | Same cohort [53] | Analyze intrathoracic and extrathoracic dissemination separately |
| Selective bottleneck | Extrathoracic subclones were enriched for SCNAs and involved more organs | Cross-habitat emigrants are a non-random clonal subset | Human lung cancer observation and CIN mechanism [53, 54] | CIN/SCNA is a candidate marker of extrathoracic dissemination |
| Metastasis-to-metastasis seeding | 60% (156/258) of metastases were seeded by another metastasis | Unidirectional radial spread becomes a multinode network | Human lung cancer [53]; prostate-cancer phylogenies [61]; registry-informed breast-cancer stochastic model [62] | An established metastasis can become a secondary source |
| Time-dependent source strength | Longer-established lesions were more likely to seed again | A stable lesion may gradually become an output node | Human lung cancer autopsy cohort [53] | Include lesion age and output signals when evaluating stable disease |
| Early lineage divergence | 25% diverged before the final dominant-clone sweep in the primary tumor | The metastatic ancestor may differ from the dominant clone in the resection specimen | 126 metastatic NSCLC cases; longitudinal TRACERx [60] | A single primary region cannot reliably recover the seeding origin |
| Polyclonal dissemination | 31.7% (40/126) of cases; associated with extrathoracic recurrence | Several primary clones contribute to the disseminating population | 126 metastatic NSCLC cases [60] | Sequencing depth and number of sampled lesions affect detection |
| Single-site sampling bias | One primary region can misclassify divergence timing; one metastasis underestimates network diversity | Sparse sampling flattens spatial structure | Multiregion and longitudinal analyses [53, 60, 107] | Integrate tissue, ctDNA, and multi-lesion imaging |
| Return migration/self-seeding | Highly metastatic populations return to primary tumors in experimental models | The primary tumor can function as both source and sink | Breast, colorectal and melanoma experimental self-seeding [116] | Direct phylogenetic validation is still needed in human lung cancer |

Note: Percentages refer to the sampling frame of each original cohort. ctDNA aggregates multi-lesion signals, with contributions shaped by lesion site, volume, perfusion, and DNA shedding.

Competition can be represented by Lotka–Volterra terms for treatment-sensitive and resistant populations, calibrated against longitudinal population measurements and experiments with different starting mixtures. Model structure, sampling design, and spatial heterogeneity determine parameter identifiability and interpretation [117, 118]. Carrying capacity is a condition-dependent parameter estimated from growth data. Absolute ctDNA concentration divided by contemporaneous tumor volume describes plasma signal per unit burden; DNA release, clearance, lesion location, and treatment affect this ratio. Table 3 links these quantities to candidate observations and estimation requirements.

## 6.3 Organ-specific selection and niche-enabled adaptation

Every lesion in the network occupies a specific organ. Brain, liver, and bone select incoming cells through distinct vascular barriers, immune baselines, ECM, and metabolic resources and continue to remodel cell state after colonization. Large-scale pan-cancer sequencing has identified non-random associations between genomic alterations and metastatic sites [119]. The "seed and soil" hypothesis thereby acquires a more specific mechanistic meaning: organ distribution is jointly determined by cancer-cell programs, routes of arrival, and host habitat [120, 121]. Macrophages also assume different functions during detachment, circulation, colonization, dormancy, and reawakening [122].

Liver metastasis connects organ-level ecology to systemic immunity. In NSCLC and melanoma patient cohorts, liver involvement was associated with reduced benefit from immune-checkpoint blockade. Mouse experiments linked this phenotype to hepatic recruitment of monocyte-derived FasL-positive macrophages that eliminated Fas-positive CD8-positive T cells [123]. This mechanism explains how one metastatic habitat can weaken immune pressure elsewhere. Clinical analyses should record liver burden and myeloid composition alongside the total extent of metastatic disease.

**Table 3.** Proposed operational measures and model parameters of the lung cancer ecosystem

| Quantity | Definition and units | Candidate observations | Estimation and interpretation |
|---|---|---|---|
| Lesion burden $N_i$ or $V_i$ | $N_i$: viable cell count; $V_i$: imaging volume, $cm^3$ | Serial imaging; quantitative tissue measurements | Consistent measurement rules; explicit calibration between volume and cell count |
| Local net growth $g_i$ | Local proliferation minus death; $time^{-1}$ | Burden trajectories; proliferation and death measurements | Joint estimation with migration; observed growth includes immigration and emigration |
| Carrying capacity K | Condition-dependent population scale; same units as modeled burden | Growth trajectories; habitat and treatment measurements | Model-estimated; parameter uncertainty and identifiability assessment |
| Habitat quality $H_i$ | Vector of perfusion, hypoxia, immune access, ECM and drug exposure | Functional imaging; spatial pathology; pharmacologic measurements | Retain component-specific units; no arbitrary composite score |
| Cell export $E_{ij} = e_{ij} N_i$ | Cells leaving i toward j per unit time; cells $time^{-1}$ | CTC measurements; regional blood sampling; lineage data | Calibrate proxy observations; separate departure, survival and establishment |
| Occupancy transitions $c_i$ and $\varepsilon_i$ | Conditional 0→1 and 1→0 probabilities over $\Delta t$; dimensionless | Serial states of predefined anatomical units | Biological occupancy $X_i$ versus detectable disease $Y_i$; record thresholds, treatment and censoring |
| Competition $\alpha_{RS}$ and $\alpha_{SR}$ | Population interaction coefficients; dimensionless under a common burden unit | Frequency-dependent co-culture; population-resolved time courses | $\alpha_{RS}$: S effect on R; $\alpha_{SR}$: R effect on S; treatment-specific calibration |
| Plasma signal per burden Q | Absolute ctDNA concentration / concurrent tumor volume; molecules $mL^{-1}$ $cm^{-3}$ | Absolute tumor-derived DNA concentration; multi-lesion volume | Release and clearance effects; detection-limit censoring; undefined at zero volume |
| Network edge i→j | Inferred ancestral or seeding relationship; no flux unit | Multi-region sequencing; longitudinal phylogenetic reconstruction | Sampling-dependent relationship; distinguish lineage ancestry from measured cell transport |

Note: The equations provide a proposed measurement framework rather than patient-fitted parameter values. Rates use a declared common time unit. Cell counts and imaging volumes are kept distinct unless an explicit calibration is available.

a. $N_i$ is the viable population at site i; $g_i$ is local net growth; $e_{ij}$ is the emigration rate from i toward j; $p_{ji}$ is the dimensionless probability of successful transfer from j to i. $g_i$ and $e_{ij}$ have units $time^{-1}$. A demographic sink has local losses replenished by immigration [115].

$$dN_i/dt = g_i N_i - \Sigma_{j \neq i} e_{ij} N_i + \Sigma_{j \neq i} p_{ji} e_{ji} N_j$$

b. For each predefined unit, $X_i = 0$ denotes biological absence and $X_i = 1$ a viable population. Matrix rows give the current state and columns the next state in the order 0, 1. $c_i$ and $\varepsilon_i$ are probabilities conditional on the current state over $\Delta t$, not instantaneous rates; they can depend on the network and treatment. $\pi_i = Pr(X_i = 1)$; $\pi_i$ values need not sum to one. Clinical $Y_i$ instead records detectable disease, with separate appearance and disappearance probabilities. Detection thresholds, examination intervals and missing observations must be specified [114].

$$P_i(t, \Delta t) = \begin{pmatrix} 1 - c_i & c_i \\ \varepsilon_i & 1 - \varepsilon_i \end{pmatrix}$$

$$\pi_i(t + \Delta t) = [1 - \pi_i(t)]\, c_i + \pi_i(t)\, [1 - \varepsilon_i]$$

c. S and R denote populations classified by sensitivity to the specified treatment; S, R, $K_S$ and $K_R$ share a burden unit. r and d(u) have units $time^{-1}$, and u denotes treatment exposure. $\alpha_{RS}$ measures the effect of S on R; $\alpha_{SR}$ measures the reverse effect. Positive coefficients indicate competition. Model calibration requires informative longitudinal data and uncertainty assessment [117, 118]. Drug-tolerant persister states require explicit state-transition terms when included.

$$dS/dt = r_S S [1 - (S + \alpha_{SR} R)/K_S] - d_S(u) S$$

$$dR/dt = r_R R [1 - (R + \alpha_{RS} S)/K_R] - d_R(u) R$$

d. $C_{ctDNA}$ is an absolute tumor-derived DNA concentration, not variant allele fraction; $V_{tumor}$ is concurrent measured tumor volume. Q is a signal-to-burden ratio, not a cellular export or DNA shedding rate. Below-detection measurements are censored rather than set to zero.

$$Q = C_{ctDNA}/V_{tumor}$$

**Table 4.** Filtering, niche-enabled adaptation, and systemic effects in liver, brain, and bone metastases

| Organ | Entry filter | Host resources | Evolutionary outcome | Systemic effect | Evidence base | Clinical implication |
|---|---|---|---|---|---|---|
| Liver | Immune tolerance; myeloid dominance | FasL+ macrophages; tolerogenic inflammation | Local selection and habitat use | Systemic effector-T-cell depletion in models; reduced ICI benefit in patient cohorts | NSCLC/melanoma clinical association; mouse FasL–T-cell mechanism [123] | Assess liver burden and myeloid composition alongside total metastatic burden |
| Brain | Blood-brain barrier; metabolic and glial adaptation | PCDH7-Cx43 signaling; glial and metabolic resources | Strong bottleneck selection followed by reprogramming | Evolutionary branch separated from extracranial disease | Patient branching/omics; breast and lung cancer gap-junction experiments with paired patient observations [124-126, 128] | Profile brain lesions separately and optimize intracranial drug exposure |
| Bone | Mineralized matrix; hypoxia; continuous bone remodeling | Resorption-associated growth factors; EZH2-linked plasticity | Clonal selection and niche-enabled adaptation | EZH2-linked secondary dissemination demonstrated in breast/prostate experiments | Breast/prostate experimental mechanism [139]; primary NSCLC CAF association, 14 patients [140] | Paired bone/primary samples to test EZH2-linked reseeding in human NSCLC and SCLC |

Note: Clonal selection and phenotypic reprogramming after arrival can coexist. The evidence column separates patient observations from experimental mechanisms. The NSCLC CAF study sampled primary lung tumors grouped by metastatic site [140]. ICI, immune-checkpoint inhibitor.

Brain metastasis is selected by the blood-brain barrier and must adapt to a neural-glial ecosystem. Paired primary and brain metastases show branched evolution and potentially actionable alterations [124], while single-cell, spatial, and multi-omic studies in lung cancer reveal distinct cellular composition and metabolic vulnerabilities in brain lesions [125-127]. Cancer cells entering the brain can also hijack mature host structures. PCDH7-Cx43 gap junctions mediate signaling between tumor cells and astrocytes, whereas endothelial cells and pericytes participate in intracranial immune regulation [128, 129].

Lung cancer subtypes exploit intracranial resources in different ways. Small-cell lung cancer models reveal developmental-like interactions with astrocytes [130], while astrocyte-derived IL-11 upregulates tumor PD-L1 in experimental EGFR-mutant NSCLC [131]. GABA metabolic reprogramming and LCN2-mediated reciprocal signaling link nutrient use to bidirectional communication [132, 133]. Brain lesions evolve under these local pressures and respond differently to treatment [134, 135]. Experimental lung tumors also suppress systemic antitumor immunity through a sensory-sympathetic neural circuit, connecting interorgan neural signaling to tumor ecology [136]. Patient-derived single-cell analyses associated HIF2A activity with inferred CAF-state transitions in lung cancer brain metastases [137]. Patient brain-metastasis profiling linked TKI exposure to altered *CTLA4* expression in T cells; CTLA-4 blockade combined with TKIs improved efficacy in syngeneic EGFR-mutant mouse models [138].

The bone niche can reshape disseminating capacity after colonization. Breast and prostate cancer experiments identify bone-induced EZH2-dependent epigenetic reprogramming as a route to enhanced secondary dissemination [139]. In NSCLC, Xu et al. analyzed primary lung tumors from 14 untreated patients grouped by metastatic site and identified differences in CAF composition [140]. The patient data connect primary stromal organization with metastatic distribution, while the bone experiments establish a mechanism for renewed dissemination. Paired bone and primary specimens with longitudinal clonal analysis are priorities for testing EZH2-linked secondary dissemination directly in human NSCLC and SCLC. Table 4 compares organ-entry filters, host resources, evolutionary outcomes, and systemic effects in liver, brain, and bone.

### 6.4 Return migration and self-seeding

Human migration provides a structural parallel for return flows: ancient genomes show that migration back into previously occupied regions reshaped population structure [141]. Human NSCLC phylogenies identify metastases as sources of further metastatic seeding [53, 60]. Self-seeding experiments in breast cancer, colorectal cancer, and melanoma establish a complementary route in which circulating cells return to an existing tumor and promote growth, angiogenesis, and stromal recruitment [116].

In the Hessey cohort, primary-tumor resection preceded radiological detection of metastases, so reconstructed human routes concern subsequent dissemination rather than return to an intact primary lesion [53]. Longitudinal sampling of an unresected primary and distant lesions would allow direct testing of self-seeding in patients with NSCLC or SCLC. Human return migration combines sexual recombination and ancestry mixing; returning tumor clones compete, coexist, and remodel their shared habitat.

Lesion roles change as local populations grow, receive immigrants, and export new founders. Reconstructing these flows identifies where dissemination begins, which sites act as intermediates, and which established lesions continue to seed. Anatomical location and size alone do not capture this evolving contribution.

## 7. Ecological remodeling and feedback control under treatment selection

### 7.1 Treatment bottlenecks, refugia, and the relapse ecosystem

Environmental change and selective removal can rapidly reorganize populations. Peppered-moth melanism and fisheries-associated shifts in cod maturation illustrate changes in phenotype frequencies under altered selection [142, 143]. Cancer treatment couples selective killing to DNA damage, cell-state transitions, immune changes, and matrix remodeling. Table 1 frames this phase through directional selection, competitive release, and pharmacokinetic, anatomical, and physiological refugia [45].

Fig. 4A begins with a sensitive majority, rare resistant clones, and reversible DTPs. Therapy removes most sensitive cells and creates a bottleneck that releases space, nutrients, and growth signals for survivors. Radiologic nadir records burden, not the evolutionary potential of residual cells.

Residual cells survive within overlapping refugia. Poorly perfused matrix reduces drug exposure, the blood-brain barrier limits the entry of some agents, and reversible DTP states reduce treatment sensitivity [45]. Anatomical protection and cell-state tolerance can coexist in the same lesion, allowing surviving populations time to adapt under continuing treatment pressure.

DTPs survive through reversible cell-state changes, whereas resistant clones maintain low sensitivity to a specified treatment. EGFR inhibition can induce APOBEC3A in persisters, increasing DNA damage, mutations, structural variation, and stable resistance [63]. Treatment selects existing variation and can alter the production of new variation in survivors. Drug tolerance describes a persistence state, resistance describes treatment sensitivity, and relapse records renewed disease growth; several routes connect these distinct levels.

Therapy also remodels the relapse niche through paracrine signals and lineage plasticity. Osimertinib can activate a TGF-β2-dependent secretory program that promotes adenocarcinoma growth and metastasis [64], while small-cell transformation bypasses EGFR targeting by changing lineage identity [65]. Liquid biopsy tracks genomic events but cannot establish histologic transformation; suspicious clinical or imaging changes require tissue. Fig. 4A integrates these routes into an immune-cold, regrowth- and dissemination-competent relapse ecosystem.

### 7.2 Immune editing, lineage switching, and dormant-cell reawakening

Immunotherapy restores antitumor immunity while selecting subclones with HLA loss, antigen loss, or defective presentation [74, 75]. Deep longitudinal analysis of EGFR-mutant lung cancer documented loss of an EGFR exon 19 deletion, small-cell transformation, and loss of vaccine-targeted neoantigens. When integrated with TRACERx, the study also showed that mutations acquired before whole-genome doubling (WGD) more often remain clonal and are less readily lost during metastasis [66]. Clonal pre-WGD alterations usually occupy several chromosome copies, imposing a greater chromosomal cost on complete loss and making them candidate immune targets with a high cost of escape. Target expression, antigen presentation, and immunogenicity will still determine treatment efficacy.

Different lesions can follow different escape routes under targeted therapy and immunotherapy. Target loss or bypass activation may sustain one lesion, while HLA loss, immune exclusion, or lineage switching supports another. Mixed responses can reflect several lesion-specific resistance processes. Multi-lesion imaging, ctDNA, and biopsy of a progressing lesion provide complementary information about the populations driving systemic progression.

Treatment reshapes surviving cancer cells and the routes available to them. In breast cancer models, chemotherapy increased tumor microenvironment of metastasis (TMEM)-associated intravasation, with related changes observed in paired human breast specimens [144]. Inflammation-induced NETs awakened dormant breast cancer cells in mouse lungs [89], whereas tumor-derived type III collagen maintained dormancy in mammary and head-and-neck tumor systems [90]. These mechanisms connect vascular access, immune activity, and matrix organization to residual-cell behavior after treatment [67]. Testing treatment-associated TMEM intravasation in patients with NSCLC or SCLC requires paired pretreatment and post-treatment lung specimens.

Relapse can arise through expansion of pre-existing resistant clones, further evolution of DTPs, reawakening of dormant cells, or lineage switching. Fig. 4A places these routes within the treatment bottleneck, where their different timescales create distinct opportunities for intervention. At relapse, tissue biopsy identifies histologic change, sequencing resolves genetic resistance, and imaging locates progressing lesions. Spatial and functional measurements can then assess the habitat sustaining those populations.

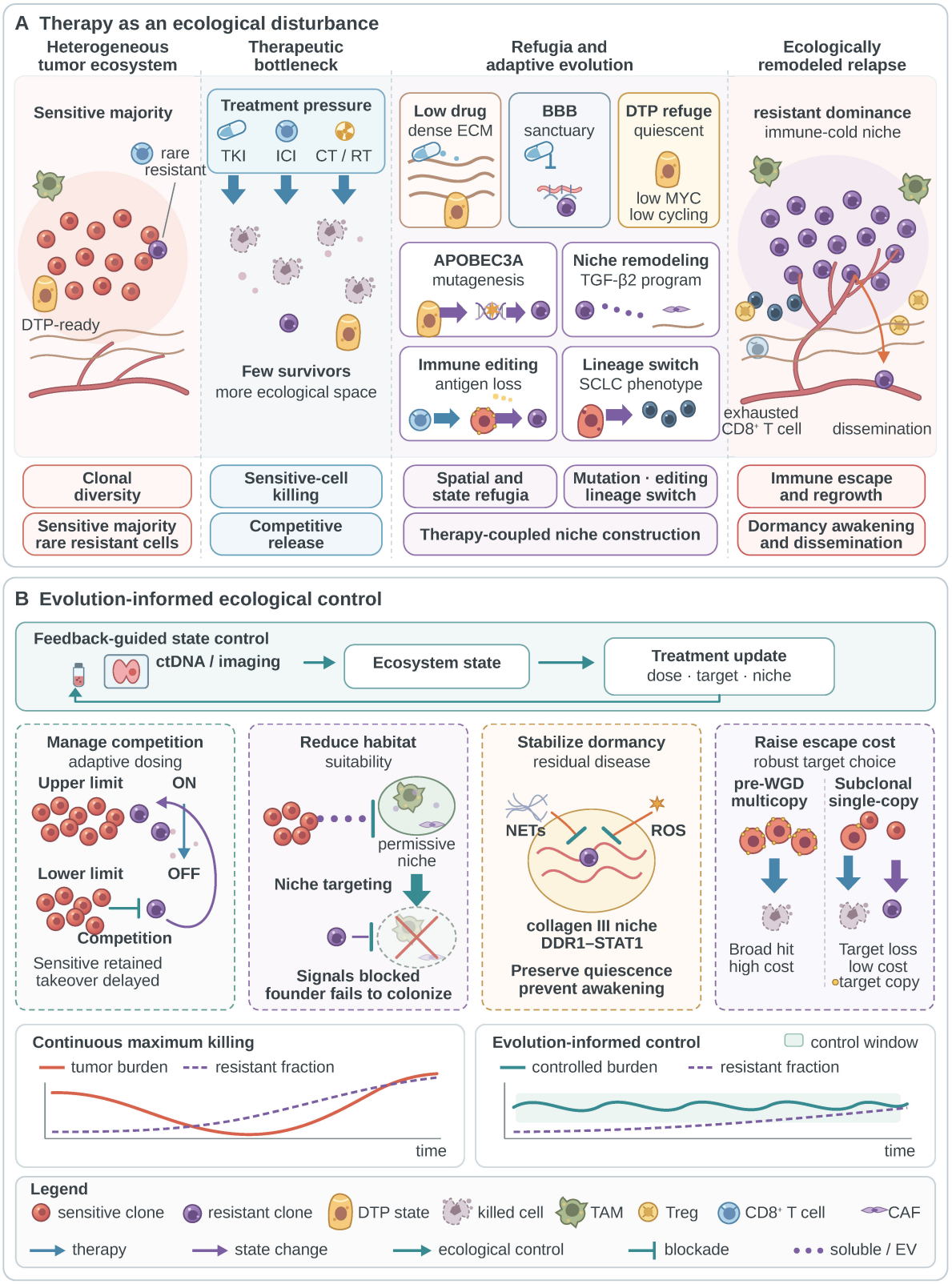



**Figure 4.** Therapy as an ecological selection pressure and evolution-informed control of lung cancer. (A) The pretreatment ecosystem contains a sensitive majority, rare resistant clones, and reversible drug-tolerant persisters (DTPs). Targeted therapy, immune-checkpoint inhibition, and cytotoxic or local treatment impose a bottleneck while leaving survivors in pharmacokinetic, anatomical, and physiological refugia. Treatment can couple to APOBEC3A-mediated mutagenesis, TGF-β2-dependent niche remodeling, immune editing, and lineage switching, enriching a resistant, immune-cold, dissemination-competent relapse ecosystem. (B) Evolution-informed control uses longitudinal circulating tumor DNA (ctDNA) and multi-lesion imaging to update treatment according to ecosystem state. Strategies include preserving sensitive competitors through adaptive dosing, reducing supportive-niche suitability, stabilizing residual-cell dormancy, and targeting clonal alterations acquired before whole-genome doubling (pre-WGD), whose loss carries a greater evolutionary cost. The trajectories schematically contrast rapid regression and resistant rebound under continuous maximum killing with feedback-guided control that seeks to maintain tumor burden within a tolerable window and delay resistant takeover. Abbreviations: BBB, blood-brain barrier; CT, chemotherapy; RT, radiotherapy; ICI, immune-checkpoint inhibitor; TKI, tyrosine kinase inhibitor; SCLC, small-cell lung cancer. Dashed boxes denote proposed strategies for investigation in lung cancer. Panel B integrates competition control with predefined systemic and CNS safety thresholds for prospective evaluation in NSCLC.

### 7.3 From maximum killing to feedback-guided ecological control

Adaptive therapy seeks to delay resistant takeover by retaining treatment-sensitive competitors and adjusting treatment exposure to tumor dynamics [145]. A pilot study in metastatic castration-resistant prostate cancer provided clinical proof of concept [68]. In cocultures of gefitinib-sensitive PC9 cells and an experimentally evolved resistant population, growth and competitive outcomes depended on relative population frequencies and drug exposure [118]. Competition-based control in NSCLC requires demonstrable suppressive interactions under the relevant treatment conditions and a clinically acceptable tumor burden.

A single-center prospective study explored biomarker-guided TKI holidays after TKI treatment and local consolidative therapy in 60 selected patients with driver-positive lung adenocarcinoma, predominantly EGFR-mutant (56/60). Cessation required no radiographically detectable lesions, undetectable plasma ctDNA, and normal serum carcinoembryonic antigen (CEA). Prior TKIs were restarted at the first occurrence of detectable ctDNA, elevated CEA, or RECIST progression [146]. This study provides preliminary clinical support for de-escalation after deep response through surveillance and timely treatment resumption. It addresses residual-disease monitoring rather than testing the preservation of sensitive competitors.

Safety depends on disease state. In patients with EGFR-mutant lung cancer and acquired resistance to gefitinib or erlotinib, protocol-mandated withdrawal was followed by disease flare in 14 of 61 patients, at a median of 8 days, requiring hospitalization or causing death; central nervous system (CNS) or pleural involvement and shorter time to progression on the initial TKI were associated with flare [147]. Intracranial progression despite undetectable plasma ctDNA in the Dong study further supports dedicated brain imaging during surveillance [146].

For initial studies of complete TKI interruption, we propose prioritizing TKI-treated EGFR-mutant NSCLC with an indolent oligometastatic course, durable control, no radiographically detectable disease after local consolidation, and reliable surveillance. Rapidly progressive driver-mutant disease, threatened organ function, active or symptomatic CNS disease, leptomeningeal involvement, or a history of withdrawal flare should exclude patients from these initial studies. Previously treated, stable brain metastases require separate stratification and serial brain magnetic resonance imaging (MRI). Selection should reflect disease kinetics and organ risk as well as driver genotype. SCLC requires a separate disease-specific design. Protocols should prespecify treatment-resumption rules and assess intracranial and systemic progression, symptoms, and urgent interventions.

Fig. 4B links longitudinal ctDNA and multi-lesion imaging to decisions about treatment intensity, combinations, local therapy, and niche targeting. Feedback rules require lesion-specific safety thresholds, account for measurement delays, and trigger prompt reassessment when CNS progression or organ compromise emerges. Plasma signals, imaging, and tissue measurements contribute different information to these decisions.

Fig. 4B proposes three strategies that complement preservation of sensitive competitors. Reducing habitat suitability includes reversing immune exclusion, improving abnormal perfusion, and blocking organ-specific supportive signals. Stabilizing dormancy aims to prevent residual-cell reawakening. Increasing the cost of escape prioritizes clonal, multicopy, functionally important targets, among which pre-WGD alterations may offer an advantage. Preservation of sensitive competitors and these three strategies address competitive interactions, habitat support, cell state, and target architecture, respectively.

## Conclusions and future directions

An ecosystem perspective connects lung cancer genetics to the changing state of host tissue throughout disease. Chronic injury alters epithelial competition; pioneer clones remodel local immunity, metabolism, matrix, and vasculature; the invasive front develops selective permeability; and successive bottlenecks filter the cells that establish distant populations. Established metastases continue to evolve and seed within a multi-lesion network, which treatment then reshapes. The mangrove ecotone focuses attention on boundary permeability, while human migration highlights founder sampling and the emergence of secondary sources. Both perspectives direct treatment research toward local habitat control and continuing dissemination between lesions.

During lung cancer initiation, the selective environment created by damaged tissue determines whether abnormal clones breach homeostatic constraints. At distant sites, organ selection and niche remodeling reshape the genetic composition, cell states, and treatment responses of arriving populations. Some established lesions become new seeding sources. Durable control depends on sensitive cells, resistant clones, DTPs, host immunity, and organ habitat as well as the reduction in tumor burden.

These operational definitions provide a starting point for reproducible ecosystem measurements. Multiregion tissue sampling, longitudinal ctDNA, and multi-lesion imaging can reconstruct interlesional lineages and track changes in seeding contributions. Spatial multi-omics, metabolic imaging, and drug-distribution measurements add oxygenation, nutrient availability, immune access, and local exposure. Prospective studies should evaluate which combinations yield identifiable model parameters and clinically useful predictions across disease states.

Treatment studies should record tumor burden, clonal structure, and microenvironmental change together. Prospective lung cancer trials can compare continuous dosing, intermittent schedules, and feedback-guided regimens in populations stratified by disease kinetics, organ risk, and measured competitive interactions. Prespecified resumption rules and intracranial surveillance are essential to evaluating treatment interruption. Target prioritization should incorporate clonality, WGD timing, copy number, antigen presentation, and the cost of target loss. Local-therapy studies can ask whether treating a lesion reduces further seeding or systemic signals and changes the behavior of the remaining network.

Paired patient specimens and longitudinal studies can connect experimentally established mechanisms to dissemination and recurrence in lung cancer. Priorities include niche-enabled secondary seeding, treatment-associated intravasation, and the persistence of dormant populations. Linking these mechanisms to measured cell states, habitat features, and clinical outcomes will support treatment strategies that control the evolving ecosystem as well as its visible burden.

## Abbreviations

ACKR1: atypical chemokine receptor 1; ACVR1: activin A receptor type 1; APOBEC3A: apolipoprotein B mRNA-editing enzyme catalytic polypeptide-like 3A; AT1: alveolar type 1 cell; AT2: alveolar type 2 cell; BBB: blood-brain barrier; BM: basement membrane; BMP: bone morphogenetic protein; CAF: cancer-associated fibroblast; CARM1: coactivator-associated arginine methyltransferase 1; CCL2: C-C motif chemokine ligand 2; CCR2: C-C motif chemokine receptor 2; CD8+: cluster of differentiation 8-positive; CEA: carcinoembryonic antigen; CIN: chromosomal instability; CNS: central nervous system; CT: Y-chromosome paternal haplogroup CT in Fig. 3A or chemotherapy in Fig. 4; CTC: circulating tumor cell; ctDNA: circulating tumor DNA; CTLA-4: cytotoxic T-lymphocyte-associated protein 4 (gene symbol *CTLA4*); CXCL12: C-X-C motif chemokine ligand 12; CXCR4: C-X-C motif chemokine receptor 4; DATP: damage-associated transient progenitor; DDR1: discoidin domain receptor 1; DTP: drug-tolerant persister; ECM: extracellular matrix; EGFR: epidermal growth factor receptor; EPAS1: endothelial PAS domain protein 1; EV: extracellular vesicle; EZH2: enhancer of zeste homolog 2; FAK: focal adhesion kinase; GABA: gamma-aminobutyric acid; GZMB: granzyme B; HIF2A: hypoxia-inducible factor 2 alpha; HLA: human leukocyte antigen; ICD: immunogenic cell death; ICI: immune-checkpoint inhibitor; IFN-γ: interferon gamma; IL: interleukin; KRAS: Kirsten rat sarcoma viral oncogene homolog; LCN2: lipocalin 2; LKB1: liver kinase B1; LOX: lysyl oxidase; LOXL2: lysyl oxidase-like 2; MCT4: monocarboxylate transporter 4; MDSC: myeloid-derived suppressor cell; MMP: matrix metalloproteinase; MRI: magnetic resonance imaging; NET: neutrophil extracellular trap; NK: natural killer; NR2F2: nuclear receptor subfamily 2 group F member 2; NR4A: nuclear receptor subfamily 4 group A; NSCLC: non-small-cell lung cancer; PD-1: programmed cell death protein 1; PD-L1: programmed death-ligand 1; PEACE: Posthumous Evaluation of Advanced Cancer Environment; PI3K: phosphoinositide 3-kinase; PM2.5: particulate matter with an aerodynamic diameter of 2.5 μm or less; POSTN: periostin; RECIST: Response Evaluation Criteria in Solid Tumors; RNS: reactive nitrogen species; ROS: reactive oxygen species; RT: radiotherapy; S100A8: S100 calcium-binding protein A8; SASP: senescence-associated secretory phenotype; SCLC: small-cell lung cancer; SCNA: somatic copy-number alteration; SLC2A3: solute carrier family 2 member 3; SLC43A2: solute carrier family 43 member 2; STAS: spread through air spaces; STAT1: signal transducer and activator of transcription 1; TAM: tumor-associated macrophage; TAZ: transcriptional coactivator with PDZ-binding motif (WWTR1); TGF-β: transforming growth factor beta; TKI: tyrosine kinase inhibitor; TMEM: tumor microenvironment of metastasis; TNF: tumor necrosis factor; TOX: thymocyte selection-associated high mobility group box; TOX2: TOX high mobility group box family member 2; TRACERx: Tracking Cancer Evolution through Therapy; Treg: regulatory T cell; TREM2: triggering receptor expressed on myeloid cells 2; VEGFR1: vascular endothelial growth factor receptor 1; WGD: whole-genome doubling; YAP: Yes-associated protein; ZEB1: zinc finger E-box-binding homeobox 1.

## Acknowledgements

The authors acknowledge the use of ChatGPT and Codex (OpenAI), as described in 'AI-assisted manuscript preparation and revision'. The authors take full responsibility for the final content.

## AI-assisted manuscript preparation and revision

During manuscript preparation, the authors used ChatGPT and Codex (OpenAI) to assist with translation of the Chinese draft into English, language and structural revision, and preparation of draft figures. During revision, these tools were used to check translations, verify additional references, and review the revision plan. The authors reviewed and edited the content adopted in the final version and take full responsibility for the accuracy and integrity of the manuscript and figures.

## Author contributions

J.W. led the conceptualization, literature search, evidence synthesis, visualization, and preparation of the original draft. Y.D. contributed to literature appraisal, reference verification, table preparation, and manuscript revision. P.H. synthesized pharmacological and treatment-related evidence, prepared the tables, and revised the manuscript. Y.C. evaluated the clinical implications of the ecological framework and critically revised the manuscript. S.C. contributed to conceptual refinement, supervision, project administration, and critical revision. All authors read and approved the final manuscript.

## Competing Interests

The authors have declared that no competing interest exists.

## References


1. Kim S, Lee Y, Song BR, Sim H, Kang EH, Hwang M, et al. Drug response of patient-derived lung cancer cells predicts clinical outcomes of targeted therapy. Cancers (Basel). 2024; 16: 778.
2. Fisher R, Pusztai L, Swanton C. Cancer heterogeneity: implications for targeted therapeutics. Br J Cancer. 2013; 108: 479-485.
3. Attili I, Tarantino P, Passaro A, Stati V, Curigliano G, de Marinis F. Strategies to overcome resistance to immune checkpoint blockade in lung cancer. Lung Cancer. 2021; 154: 151-160.
4. Hanahan D. Hallmarks of cancer: New dimensions. Cancer Discov. 2022; 12: 31-46.
5. Greaves M, Maley CC. Clonal evolution in cancer. Nature. 2012; 481: 306-313.
6. Sikkema L, Ramírez-Suástegui C, Strobl DC, Gillett TE, Zappia L, Madissoon E, et al. An integrated cell atlas of the lung in health and disease. Nat Med. 2023; 29: 1563-1577.
7. Firsova AB, Marco Salas S, Kuemmerle LB, Abalo XM, Sountoulidis A, Larsson L, et al. Spatial single-cell atlas reveals regional variations in healthy and diseased human lung. Nat Commun. 2025; 16: 9745.
8. Madissoon E, Oliver AJ, Kleshchevnikov V, Wilbrey-Clark A, Polanski K, Richoz N, et al. A spatially resolved atlas of the human lung characterizes a gland-associated immune niche. Nat Genet. 2023; 55: 66-77.
9. Quail DF, Joyce JA. Microenvironmental regulation of tumor progression and metastasis. Nat Med. 2013; 19: 1423-1437.
10. Zeng P, Li HF, Shu WB, Zhang J, Zhao TC, Hu JW, et al. Single-cell and spatial transcriptomics reveal that the CXCL12-CXCR4 axis drives the immune-desert phenotype in small cell lung cancer by recruiting immunosuppressive CXCR4(+) neutrophils and S100A8(+) monocytes. J Immunother Cancer. 2026; 14: e013867.
11. Enfield KSS, Colliver E, Lee C, Magness A, Moore DA, Sivakumar M, et al. Spatial architecture of myeloid and T cells orchestrates immune evasion and clinical outcome in lung cancer. Cancer Discov. 2024; 14: 1018-1047.
12. Odling-Smee FJ, Laland KN, Feldman MW. Niche construction: The neglected process in evolution. Princeton, USA: Princeton University Press; 2003.
13. Matthews B, De Meester L, Jones CG, Ibelings BW, Bouma TJ, Nuutinen V, et al. Under niche construction: An operational bridge between ecology, evolution, and ecosystem science. Ecol Monogr. 2014; 84: 245-263.
14. Tansley AG. The use and abuse of vegetational concepts and terms. Ecology. 1935; 16: 284-307.
15. Richter DD, Billings SA. 'One physical system': Tansley's ecosystem as Earth's critical zone. New Phytol. 2015; 206: 900-912.
16. Guo G, Zhang H. A mechanism of food-web complexity emergence under multiple environmental drivers. Ecol Evol. 2026; 16: e73138.
17. Parker AL, Cox TR. The role of the ECM in lung cancer dormancy and outgrowth. Front Oncol. 2020; 10: 1766.
18. Kim J, Tanner K. Recapitulating the tumor ecosystem along the metastatic cascade using 3D culture models. Front Oncol. 2015; 5: 170.
19. Liu L, Yang L, Li H, Shang T, Liu L. The tumor microenvironment in lung cancer: Heterogeneity, therapeutic resistance and emerging treatment strategies (Review). Int J Oncol. 2026; 68: 11.
20. Chandra R, Ehab J, Hauptmann E, Gunturu NS, Karalis JD, Kent DO, et al. The current state of tumor microenvironment-specific therapies for non-small cell lung cancer. Cancers (Basel). 2025; 17: 1732.
21. Shen Y, Goncharov DA, Pena A, Baust J, Chavez Barragan A, Ray A, et al. Cross-talk between TSC2 and the extracellular matrix controls pulmonary vascular proliferation and pulmonary hypertension. Sci Signal. 2022; 15: eabn2743.
22. Feng Y, Jiang Y, Yang L, Lu D, Li N, Zhang Q, et al. Targeting CAFs and extracellular matrix (ECM) in lung cancer: Potential of adjuvants and nanoparticles. Bioorg Chem. 2025; 162: 108586.
23. Mao X, Cao X, Qian L, Gao M, Zhang N, Huang M, et al. Vascular abnormalization confers tumor resistance to antiangiogenic therapy via downregulating angiostatic factors. Breast Cancer Res. 2026; 28: 59.
24. Hao S, Ai D, Wang Q, Zhang X, Ma X, Tseng I, et al. PD-1 inhibitor improves radiosensitivity by tumor vessel normalization. Br J Cancer. 2026; 134: 820-830.
25. Huo J, Guan J, Li Y. Metabolism reprogramming signature associated with stromal cells abundance in tumor microenvironment improve prognostic risk classification for gastric cancer. BMC Gastroenterol. 2022; 22: 364.
26. Ding Y, Tian Y, Ren W, Hu X, Li M, Liu B, et al. SLC2A3-mediated lactate metabolism promotes lung cancer bone metastasis by modulating p53 lactylation and immune evasion. Adv Sci (Weinh). 2026; 13: e16622.
27. Wang Z, Yan N, Sheng H, Xiao Y, Sun J, Cao C. Single-cell transcriptomic analysis reveals an immunosuppressive network between POSTN CAFs and ACKR1 ECs in TKI-resistant lung cancer. Cancer Genomics Proteomics. 2024; 21: 65-78.
28. Deng H, Liu Q, Tian Z, Liu G, Wang S, Liang D, et al. Spatial transcriptomics uncovers immune-cell plasticity and dedifferentiation signatures in aggressive lung adenocarcinoma subtypes. Front Immunol. 2025; 16: 1620886.
29. Zhou S, Guo Y, Cheng R, Zhang Q, Xing Y, Geng Y, et al. NR2F2 in cancer-associated fibroblasts drives immune microenvironment remodeling and promotes lung adenocarcinoma progression. Front Immunol. 2026; 17: 1776008.
30. Wang M, Song Z, Yuan H, Liu C, Wang W, Yang N, et al. Protumor macrophage polarization mediated by BMP2/4-ACVR1 signaling orchestrates an immunosuppressive microenvironment during tumor initiation. Cancer Res. 2026; 86: 954-971.
31. Meng F, Sun Y, Li J, Xu L. Single-cell and spatial transcriptome landscapes reveal the spatial immune defense pattern shared by primary and brain metastatic lung adenocarcinoma. J Thorac Dis. 2025; 17: 9927-9942.
32. Storz JF, Cheviron ZA. Physiological genomics of adaptation to high-altitude hypoxia. Annu Rev Anim Biosci. 2021; 9: 149-171.
33. Jing X, Yang F, Shao C, Wei K, Xie M, Shen H, et al. Role of hypoxia in cancer therapy by regulating the tumor microenvironment. Mol Cancer. 2019; 18: 157.
34. Hill W, Lim EL, Weeden CE, Lee C, Augustine M, Chen K, et al. Lung adenocarcinoma promotion by air pollutants. Nature. 2023; 616: 159-167.
35. Choi J, Park JE, Tsagkogeorga G, Yanagita M, Koo BK, Han N, et al. Inflammatory signals induce AT2 cell-derived damage-associated transient progenitors that mediate alveolar regeneration. Cell Stem Cell. 2020; 27: 366-382.e7.
36. Falvo DJ, Grimont A, Zumbo P, Fall WB, Yang JL, Osterhoudt A, et al. A reversible epigenetic memory of inflammatory injury controls lineage plasticity and tumor initiation in the mouse pancreas. Dev Cell. 2023; 58: 2959-2973.e7.
37. Park Y, Lee D, Lee JE, Park HS, Jung SS, Park D, et al. The matrix stiffness coordinates cell proliferation and PD-L1 expression via YAP in lung adenocarcinoma. Cancers (Basel). 2024; 16: 598.
38. Frankell AM, Dietzen M, Al Bakir M, Lim EL, Karasaki T, Ward S, et al. The evolution of lung cancer and impact of subclonal selection in TRACERx. Nature. 2023; 616: 525-533.
39. Casanova-Acebes M, Dalla E, Leader AM, LeBerichel J, Nikolic J, Morales BM, et al. Tissue-resident macrophages provide a pro-tumorigenic niche to early NSCLC cells. Nature. 2021; 595: 578-584.
40. Katzenelenbogen Y, Sheban F, Yalin A, Yofe I, Svetlichnyy D, Jaitin DA, et al. Coupled scRNA-seq and intracellular protein activity reveal an immunosuppressive role of TREM2 in cancer. Cell. 2020; 182: 872-885.e19.
41. Seo H, Chen J, González-Avalos E, Samaniego-Castruita D, Das A, Wang YH, et al. TOX and TOX2 transcription factors cooperate with NR4A transcription factors to impose CD8(+) T cell exhaustion. Proc Natl Acad Sci U S A. 2019; 116: 12410-12415.

42. Chen G, Huang AC, Zhang W, Zhang G, Wu M, Xu W, et al. Exosomal PD-L1 contributes to immunosuppression and is associated with anti-PD-1 response. Nature. 2018; 560: 382-386.
43. Poggio M, Hu T, Pai CC, Chu B, Belair CD, Chang A, et al. Suppression of exosomal PD-L1 induces systemic antitumor immunity and memory. Cell. 2019; 177: 414-427.e13.
44. Bian Y, Li W, Kremer DM, Sajjakulnukit P, Li S, Crespo J, et al. Cancer SLC43A2 alters T cell methionine metabolism and histone methylation. Nature. 2020; 585: 277-282.
45. Sharma SV, Lee DY, Li B, Quinlan MP, Takahashi F, Maheswaran S, et al. A chromatin-mediated reversible drug-tolerant state in cancer cell subpopulations. Cell. 2010; 141: 69-80.
46. Qiao M, Zhou F, Liu X, Jiang T, Wang H, Li X, et al. Targeting focal adhesion kinase boosts immune response in KRAS/LKB1 co-mutated lung adenocarcinoma via remodeling the tumor microenvironment. Exp Hematol Oncol. 2024; 13: 11.
47. Karasaki T, Moore DA, Veeriah S, Naceur-Lombardelli C, Toncheva A, Magno N, et al. Evolutionary characterization of lung adenocarcinoma morphology in TRACERx. Nat Med. 2023; 29: 833-845.
48. Faubert B, Li KY, Cai L, Hensley CT, Kim J, Zacharias LG, et al. Lactate metabolism in human lung tumors. Cell. 2017; 171: 358-371.e9.
49. Qian Y, Galan-Cobo A, Guijarro I, Dang M, Molkentine D, Poteete A, et al. MCT4-dependent lactate secretion suppresses antitumor immunity in LKB1-deficient lung adenocarcinoma. Cancer Cell. 2023; 41: 1363-1380.e7.
50. Peng DH, Ungewiss C, Tong P, Byers LA, Wang J, Canales JR, et al. ZEB1 induces LOXL2-mediated collagen stabilization and deposition in the extracellular matrix to drive lung cancer invasion and metastasis. Oncogene. 2017; 36: 1925-1938.
51. Tang CH, Tan TW, Fu WM, Yang RS. Involvement of matrix metalloproteinase-9 in stromal cell-derived factor-1/CXCR4 pathway of lung cancer metastasis. Carcinogenesis. 2008; 29: 35-43.
52. Stawowczyk M, Wellenstein MD, Lee SB, Yomtoubian S, Durrans A, Choi H, et al. Matrix metalloproteinase 14 promotes lung cancer by cleavage of heparin-binding EGF-like growth factor. Neoplasia. 2017; 19: 55-64.
53. Hessey S, Bunkum A, Huebner A, Haase K, Grigoriadis K, Naceur-Lombardelli C, et al. Evolutionary characterization of lung cancer metastasis. Nature. 2026; 653: 911-922.
54. Bakhoum SF, Ngo B, Laughney AM, Cavallo JA, Murphy CJ, Ly P, et al. Chromosomal instability drives metastasis through a cytosolic DNA response. Nature. 2018; 553: 467-472.
55. Pereira ER, Kedrin D, Seano G, Gautier O, Meijer EFJ, Jones D, et al. Lymph node metastases can invade local blood vessels, exit the node, and colonize distant organs in mice. Science. 2018; 359: 1403-1407.
56. Reticker-Flynn NE, Zhang W, Belk JA, Basto PA, Escalante NK, Pilarowski GOW, et al. Lymph node colonization induces tumor-immune tolerance to promote distant metastasis. Cell. 2022; 185: 1924-1942.e23.
57. Hu B, Xin Y, Hu G, Li K, Tan Y. Fluid shear stress enhances natural killer cell's cytotoxicity toward circulating tumor cells through NKG2D-mediated mechanosensing. APL Bioeng. 2023; 7: 036108.
58. Aceto N, Bardia A, Miyamoto DT, Donaldson MC, Wittner BS, Spencer JA, et al. Circulating tumor cell clusters are oligoclonal precursors of breast cancer metastasis. Cell. 2014; 158: 1110-1122.
59. Yang Y, Chen C, Lyu Y, Gololobova O, Guo X, Huang TYT, et al. HIF-1 promotes murine breast cancer brain metastasis by increasing production of integrin β3-containing extracellular vesicles. J Clin Invest. 2025; 135: e190470.
60. Al Bakir M, Huebner A, Martínez-Ruiz C, Grigoriadis K, Watkins TBK, Pich O, et al. The evolution of non-small cell lung cancer metastases in TRACERx. Nature. 2023; 616: 534-542.
61. Gundem G, Van Loo P, Kremeyer B, Alexandrov LB, Tubio JMC, Papaemmanuil E, et al. The evolutionary history of lethal metastatic prostate cancer. Nature. 2015; 520: 353-357.
62. Vitos N, Gerlee P. Model-based inference of metastatic seeding rates in *de novo* metastatic breast cancer reveals the impact of secondary seeding and molecular subtype. Sci Rep. 2022; 12: 9455.
63. Isozaki H, Sakhtemani R, Abbasi A, Nikpour N, Stanzione M, Oh S, et al. Therapy-induced APOBEC3A drives evolution of persistent cancer cells. Nature. 2023; 620: 393-401.
64. Ghosh M, Wu C, Kumar A, Nilsson M, Heymach JV, Zhao W, et al. Osimertinib activates a TGF-β2-dependent secretory program that drives lung adenocarcinoma progression. J Clin Invest. 2026; 136: e198418.
65. Huang J, Zhang Z, Cai G, Huang W, Chen YQ, Zhang J, et al. Single-cell profiling of tumor lineage plasticity and the immune microenvironment in transformed small cell lung cancer. J Transl Med. 2026; 24: 358.
66. Al Bakir M, Reading JL, Gamble S, Rosenthal R, Uddin I, Rowan A, et al. Clonal driver neoantigen loss under EGFR TKI and immune selection pressures. Nature. 2025; 639: 1052-1059.
67. Nicolas E, Kosmider B, Cukierman E, Borghaei H, Golemis EA, Borriello L. Cancer treatments as paradoxical catalysts of tumor awakening in the lung. Cancer Metastasis Rev. 2024; 43: 1165-1183.
68. Zhang J, Cunningham JJ, Brown JS, Gatenby RA. Integrating evolutionary dynamics into treatment of metastatic castrate-resistant prostate cancer. Nat Commun. 2017; 8: 1816.
69. Galluzzi L, Vitale I, Warren S, Adjemian S, Agostinis P, Buqué Martinez A, et al. Consensus guidelines for the definition, detection and interpretation of immunogenic cell death. J Immunother Cancer. 2020; 8: e000337.
70. Gorgoulis V, Adams PD, Alimonti A, Bennett DC, Bischof O, Bishop C, et al. Cellular senescence: defining a path forward. Cell. 2019; 179: 813-827.
71. Peng F, Sinjab A, Dai Y, Treekitkarnmongkol W, Yang S, Gomez Bolanos LI, et al. Multimodal spatial-omics reveal co-evolution of alveolar progenitors and proinflammatory niches in progression of lung precursor lesions. Cancer Cell. 2026; 44: 321-339.e13.
72. Yang D, Jones MG, Naranjo S, Rideout WM, Min KHJ, Ho R, et al. Lineage tracing reveals the phylodynamics, plasticity, and paths of tumor evolution. Cell. 2022; 185: 1905-1923.e25.
73. Jayathilake PG, Victori P, Pavillet CE, Lee CH, Voukantsis D, Miar A, et al. Metabolic symbiosis between oxygenated and hypoxic tumour cells: An agent-based modelling study. PLoS Comput Biol. 2024; 20: e1011944.
74. Dijkstra KK, Vendramin R, Karagianni D, Witsen M, Gálvez-Cancino F, Hill MS, et al. Subclonal immune evasion in non-small cell lung cancer. Cancer Cell. 2025; 43: 1833-1849.e10.
75. Rosenthal R, Cadieux EL, Salgado R, Al Bakir M, Moore DA, Hiley CT, et al. Neoantigen-directed immune escape in lung cancer evolution. Nature. 2019; 567: 479-485.
76. Deng Y, Hall JK, Wang Y, Kim JH, Bartolák-Suki E, Nia HT, et al. Imaging the extracellular matrix structure and remodeling in healthy, fibrotic, and emphysematous human precision-cut lung slices. Respir Res. 2026; 27: 26.
77. Planer JD, Morrisey EE. After the storm: Regeneration, repair, and reestablishment of homeostasis between the alveolar epithelium and innate immune system following viral lung injury. Annu Rev Pathol. 2023; 18: 337-359.
78. Zhang J, Liu Y. Epithelial stem cells and niches in lung alveolar regeneration and diseases. Chin Med J Pulm Crit Care Med. 2024; 2: 17-26.
79. Xiang H, Ramil CP, Hai J, Zhang C, Wang H, Watkins AA, et al. Cancer-associated fibroblasts promote immunosuppression by inducing ROS-generating monocytic MDSCs in lung squamous cell carcinoma. Cancer Immunol Res. 2020; 8: 436-450.
80. Jin C, Lagoudas GK, Zhao C, Bullman S, Bhutkar A, Hu B, et al. Commensal microbiota promote lung cancer development via γδ T cells. Cell. 2019; 176: 998-1013.e16.
81. Tsay JJ, Wu BG, Sulaiman I, Gershner K, Schluger R, Li Y, et al. Lower airway dysbiosis affects lung cancer progression. Cancer Discov. 2021; 11: 293-307.
82. Wang Y, Niu X, Cheng Y, Zhang Y, Xia L, Xia W, et al. Exosomal PD-L1 predicts response with immunotherapy in NSCLC patients. Clin Exp Immunol. 2022; 208: 316-322.
83. Panduro M, Benoist C, Mathis D. T(reg) cells limit IFN-γ production to control macrophage accrual and phenotype during skeletal muscle regeneration. Proc Natl Acad Sci U S A. 2018; 115: E2585-E2593.
84. Overacre-Delgoffe AE, Chikina M, Dadey RE, Yano H, Brunazzi EA, Shayan G, et al. Interferon-γ drives Treg fragility to promote antitumor immunity. Cell. 2017; 169: 1130-1141.e11.
85. Combes AJ, Samad B, Tsui J, Chew NW, Yan P, Reeder GC, et al. Discovering dominant tumor immune archetypes in a pan-cancer census. Cell. 2022; 185: 184-203.e19.
86. Qin X, Zhang C, Wu S, Lu J, Wang G, Li Y. Hypoxia-associated alternative polyadenylation of CARM1 and tumor microenvironment alterations in non-small cell lung cancer. Genes (Basel). 2026; 17: 505.
87. Pich O, Bernard E, Zagorulya M, Rowan A, Pospori C, Slama R, et al. Tumor-infiltrating clonal hematopoiesis. N Engl J Med. 2025; 392: 1594-1608.
88. Rehman SK, Haynes J, Collignon E, Brown KR, Wang Y, Nixon AML, et al. Colorectal cancer cells enter a diapause-like DTP state to survive chemotherapy. Cell. 2021; 184: 226-242.e21.
89. Albrengues J, Shields MA, Ng D, Park CG, Ambrico A, Poindexter ME, et al. Neutrophil extracellular traps produced during inflammation awaken dormant cancer cells in mice. Science. 2018; 361: eaao4227.
90. Di Martino JS, Nobre AR, Mondal C, Taha I, Farias EF, Fertig EJ, et al. A tumor-derived type III collagen-rich ECM niche regulates tumor cell dormancy. Nat Cancer. 2022; 3: 90-107.
91. Heidrich I, Deitert B, Werner S, Pantel K. Liquid biopsy for monitoring of tumor dormancy and early detection of disease recurrence in solid tumors. Cancer Metastasis Rev. 2023; 42: 161-182.
92. Shirvani AH, Mohammadian S, Jamshidi S, Khodabandehloo MH, Zangoie S, Moghadam RS, et al. Programmed cell death and metastatic evolution in breast cancer: the role of anoikis, necroptosis, and ferroptosis. Apoptosis. 2026; 31: 170.
93. Gilchrist DE, Ju JA, Martin SS, Vitolo MI. The pro-metastatic roles of ROS. Antioxidants (Basel). 2026; 15: 529.
94. Li P, Fan F, Zhang B, Yuan C, Liang H. Neutrophil spatiotemporal regulatory networks: dual roles in tumor growth regulation and metastasis. Biomedicines. 2025; 13: 1473.
95. Cole K, Al-Kadhimi Z, Talmadge JE. Role of myeloid-derived suppressor cells in tumor recurrence. Cancer Metastasis Rev. 2023; 42: 113-142.
96. Nasr MM, Lynch CC. How circulating tumor cluster biology contributes to the metastatic cascade: from invasion to dissemination and dormancy. Cancer Metastasis Rev. 2023; 42: 1133-1146.
97. Yang C, Liu C, Xia C, Fu L. Clinical applications of circulating tumor cells in metastasis and therapy. J Hematol Oncol. 2025; 18: 80.
98. Pontis F, Roz L, Fortunato O, Bertolini G. The metastatic niche formation: focus on extracellular vesicle-mediated dialogue between lung cancer cells and the microenvironment. Front Oncol. 2023; 13: 1116783.

99. Rodriguez-Tirado C, Sosa MS. How much do we know about the metastatic process? Clin Exp Metastasis. 2024; 41: 275-299.
100. Hublin JJ, Ben-Ncer A, Bailey SE, Freidline SE, Neubauer S, Skinner MM, et al. New fossils from Jebel Irhoud, Morocco and the pan-African origin of Homo sapiens. Nature. 2017; 546: 289-292.
101. Bergström A, Stringer C, Hajdinjak M, Scerri EML, Skoglund P. Origins of modern human ancestry. Nature. 2021; 590: 229-237.
102. Nielsen R, Akey JM, Jakobsson M, Pritchard JK, Tishkoff S, Willerslev E. Tracing the peopling of the world through genomics. Nature. 2017; 541: 302-310.
103. Ramachandran S, Deshpande O, Roseman CC, Rosenberg NA, Feldman MW, Cavalli-Sforza LL. Support from the relationship of genetic and geographic distance in human populations for a serial founder effect originating in Africa. Proc Natl Acad Sci U S A. 2005; 102: 15942-15947.
104. Green RE, Krause J, Briggs AW, Maricic T, Stenzel U, Kircher M, et al. A draft sequence of the Neandertal genome. Science. 2010; 328: 710-722.
105. Huerta-Sánchez E, Jin X, Asan, Bianba Z, Peter BM, Vinckenbosch N, et al. Altitude adaptation in Tibetans caused by introgression of Denisovan-like DNA. Nature. 2014; 512: 194-197.
106. Haak W, Lazaridis I, Patterson N, Rohland N, Mallick S, Llamas B, et al. Massive migration from the steppe was a source for Indo-European languages in Europe. Nature. 2015; 522: 207-211.
107. Abbosh C, Frankell AM, Harrison T, Kisistok J, Garnett A, Johnson L, et al. Tracking early lung cancer metastatic dissemination in TRACERx using ctDNA. Nature. 2023; 616: 553-562.
108. Gkountela S, Castro-Giner F, Szczerba BM, Vetter M, Landin J, Scherrer R, et al. Circulating tumor cell clustering shapes DNA methylation to enable metastasis seeding. Cell. 2019; 176: 98-112.e14.
109. Kaplan RN, Riba RD, Zacharoulis S, Bramley AH, Vincent L, Costa C, et al. VEGFR1-positive haematopoietic bone marrow progenitors initiate the pre-metastatic niche. Nature. 2005; 438: 820-827.
110. Grant G, Ferrer CM. The role of the immune tumor microenvironment in shaping metastatic dissemination, dormancy, and outgrowth. Trends Cell Biol. 2026; 36: 377-391.
111. Aguirre-Ghiso JA, Bravo-Cordero JJ, Guo W, Lauvau G, Sosa MS. The sleeping threat: targeting cancer dormancy to transform metastasis therapy. Nat Rev Cancer. 2026; 26: 513-533.
112. Kim DJ. Molecular and immune mechanisms governing cancer metastasis, including dormancy, microenvironmental niches, and tumor-specific programs. Int J Mol Sci. 2026; 27: 875.
113. Lambert AW, Pattabiraman DR, Weinberg RA. Emerging biological principles of metastasis. Cell. 2017; 168: 670-691.
114. Hanski I. Metapopulation dynamics. Nature. 1998; 396: 41-49.
115. Pulliam HR. Sources, sinks, and population regulation. Am Nat. 1988; 132: 652-661.
116. Kim MY, Oskarsson T, Acharyya S, Nguyen DX, Zhang XH, Norton L, et al. Tumor self-seeding by circulating cancer cells. Cell. 2009; 139: 1315-1326.
117. Cho H, Lewis AL, Storey KM, Byrne HM. Designing experimental conditions to use the Lotka–Volterra model to infer tumor cell line interaction types. J Theor Biol. 2023; 559: 111377.
118. Farrokhian N, Maltas J, Dinh M, Durmaz A, Ellsworth P, Hitomi M, et al. Measuring competitive exclusion in non-small cell lung cancer. Sci Adv. 2022; 8: eabm7212.
119. Nguyen B, Fong C, Luthra A, Smith SA, DiNatale RG, Nandakumar S, et al. Genomic characterization of metastatic patterns from prospective clinical sequencing of 25,000 patients. Cell. 2022; 185: 563-575.e11.
120. Fidler IJ. The pathogenesis of cancer metastasis: The 'seed and soil' hypothesis revisited. Nat Rev Cancer. 2003; 3: 453-458.
121. Nolan E, Kang Y, Malanchi I. Mechanisms of organ-specific metastasis of breast cancer. Cold Spring Harb Perspect Med. 2023; 13: a041326.
122. Mantovani A, Marchesi F, Di Mitri D, Garlanda C. Macrophage diversity in cancer dissemination and metastasis. Cell Mol Immunol. 2024; 21: 1201-1214.
123. Yu J, Green MD, Li S, Sun Y, Journey SN, Choi JE, et al. Liver metastasis restrains immunotherapy efficacy via macrophage-mediated T cell elimination. Nat Med. 2021; 27: 152-164.
124. Brastianos PK, Carter SL, Santagata S, Cahill DP, Taylor-Weiner A, Jones RT, et al. Genomic characterization of brain metastases reveals branched evolution and potential therapeutic targets. Cancer Discov. 2015; 5: 1164-1177.
125. Tagore S, Caprio L, Amin AD, Bestak K, Luthria K, D'Souza E, et al. Single-cell and spatial genomic landscape of non-small cell lung cancer brain metastases. Nat Med. 2025; 31: 1351-1363.
126. Duan H, Ren J, Wei S, Yang Z, Li C, Wang Z, et al. Integrated analyses of multi-omic data derived from paired primary lung cancer and brain metastasis reveal the metabolic vulnerability as a novel therapeutic target. Genome Med. 2024; 16: 138.
127. Wang Z, Wang Y, Chang M, Wang Y, Liu P, Wu J, et al. Single-cell transcriptomic analyses provide insights into the cellular origins and drivers of brain metastasis from lung adenocarcinoma. Neuro Oncol. 2023; 25: 1262-1274.
128. Chen Q, Boire A, Jin X, Valiente M, Er EE, Lopez-Soto A, et al. Carcinoma-astrocyte gap junctions promote brain metastasis by cGAMP transfer. Nature. 2016; 533: 493-498.
129. Bejarano L, Kauzlaric A, Lamprou E, Lourenco J, Fournier N, Ballabio M, et al. Interrogation of endothelial and mural cells in brain metastasis reveals key immune-regulatory mechanisms. Cancer Cell. 2024; 42: 378-395.e10.
130. Qu F, Brough SC, Michno W, Madubata CJ, Hartmann GG, Puno A, et al. Crosstalk between small-cell lung cancer cells and astrocytes mimics brain development to promote brain metastasis. Nat Cell Biol. 2023; 25: 1506-1519.
131. Tang M, Xu M, Wang J, Liu Y, Liang K, Jin Y, et al. Brain metastasis from EGFR-mutated non-small cell lung cancer: secretion of IL11 from astrocytes up-regulates PDL1 and promotes immune escape. Adv Sci (Weinh). 2024; 11: e2306348.
132. Xie M, Qin H, Liu L, Wu J, Zhao Z, Zhao Y, et al. GABA regulates metabolic reprogramming to mediate the development of brain metastasis in non-small cell lung cancer. J Exp Clin Cancer Res. 2025; 44: 61.
133. Zhu Y, Zhang J, He D, Cai H, He Y, Yuan L, et al. Lipocalin-2 drives brain metastatic progression through reciprocal tumor-microenvironment interactions in lung cancer. Signal Transduct Target Ther. 2025; 10: 417.
134. Kim MS, Lee J, Lee JE, An JH, Heo JY, Yeo MK. Brain metastasis from non-small cell lung cancer: crosstalk between cancer cells and tumor microenvironment components. Exp Mol Med. 2025; 57: 2749-2762.
135. Lu Y, Huang Y, Zhu C, Li Z, Zhang B, Sheng H, et al. Cancer brain metastasis: molecular mechanisms and therapeutic strategies. Mol Biomed. 2025; 6: 12.
136. Wei HK, Yu CD, Hu B, Zeng X, Ichise H, Li L, et al. Tumour-brain crosstalk restrains cancer immunity via a sensory-sympathetic axis. Nature. 2026; 650: 1007-1016.
137. You M, Fu M, Shen Z, Feng Y, Zhang L, Zhu X, et al. HIF2A mediates lineage transition to aggressive phenotype of cancer-associated fibroblasts in lung cancer brain metastasis. Oncoimmunology. 2024; 13: 2356942.
138. Fu M, Zhao J, Zhang L, Sheng Z, Li X, Qiu F, et al. Overcoming tyrosine kinase inhibitor resistance in lung cancer brain metastasis with CTLA4 blockade. Cancer Cell. 2024; 42: 1882-1897.e7.
139. Zhang W, Bado IL, Hu J, Wan YW, Wu L, Wang H, et al. The bone microenvironment invigorates metastatic seeds for further dissemination. Cell. 2021; 184: 2471-2486.e20.
140. Xu K, Wang H, Zou YX, Zhang HH, Wang YN, Ren XR, et al. Distinct fibroblast subpopulations associated with bone, brain or intrapulmonary metastasis in advanced non-small-cell lung cancer. Clin Transl Med. 2024; 14: e1605.
141. Skoglund P, Mathieson I. Ancient genomics of modern humans: The first decade. Annu Rev Genomics Hum Genet. 2018; 19: 381-404.
142. Van't Hof AE, Campagne P, Rigden DJ, Yung CJ, Lingley J, Quail MA, et al. The industrial melanism mutation in British peppered moths is a transposable element. Nature. 2016; 534: 102-105.
143. Olsen EM, Heino M, Lilly GR, Morgan MJ, Brattey J, Ernande B, et al. Maturation trends indicative of rapid evolution preceded the collapse of northern cod. Nature. 2004; 428: 932-935.
144. Karagiannis GS, Pastoriza JM, Wang Y, Harney AS, Entenberg D, Pignatelli J, et al. Neoadjuvant chemotherapy induces breast cancer metastasis through a TMEM-mediated mechanism. Sci Transl Med. 2017; 9: eaan0026.
145. Gatenby RA, Silva AS, Gillies RJ, Frieden BR. Adaptive therapy. Cancer Res. 2009; 69: 4894-4903.
146. Dong S, Wang Z, Zhang JT, Yan B, Zhang C, Gao X, et al. Circulating tumor DNA-guided de-escalation targeted therapy for advanced non-small cell lung cancer: a nonrandomized controlled trial. JAMA Oncol. 2024; 10: 932-940.
147. Chaft JE, Oxnard GR, Sima CS, Kris MG, Miller VA, Riely GJ. Disease flare after tyrosine kinase inhibitor discontinuation in patients with EGFR-mutant lung cancer and acquired resistance to erlotinib or gefitinib: implications for clinical trial design. Clin Cancer Res. 2011; 17: 6298-6303.